BLANKET ENGINEERING

KEYWORDS: *safety factors, fusion integral experiments, neutronics R&D*

FUSION INTEGRAL EXPERIMENTS AND ANALYSIS AND THE DETERMINATION OF DESIGN SAFETY FACTORS—II: APPLICATION TO THE PREDICTION UNCERTAINTY OF TRITIUM PRODUCTION RATE FROM THE U.S. DOE/JAERI COLLABORATIVE PROGRAM ON FUSION BLANKET NEUTRONICS

M. Z. YOUSSEF, A. KUMAR, and M. A. ABDOU
University of California, Los Angeles, School of Engineering and Applied Science
Mechanical, Aerospace, and Nuclear Engineering Department
Los Angeles, California 90095

Y. OYAMA, C. KONNO, F. MAEKAWA, Y. IKEDA, K. KOSAKO, M. NAKAGAWA, T. MORI, and H. MAEKAWA
Japan Atomic Energy Research Institute, Department of Reactor Engineering
Tokai Research Establishment, Tokai-mura, Naka-gun, Ibaraki-ken 319-11 Japan

Received January 28, 1994
Accepted for Publication July 28, 1994

Many fusion integral experiments were performed during the last decade within a well-established collaboration between the United States and Japan on fusion breeder neutronics. These experiments started in 1983 and aimed at verifying the prediction accuracy of key neutronics parameters based on the state-of-the-art neutron transport codes and basic nuclear databases. The tritium production rate (TPR) has the prime focus among other reactions. The experimental and calculational data sets of local TPR in each experiment were interpolated to give an estimate of the prediction uncertainty, u_i, and the standard deviation, σ_i of the line-integrated TPR, a quantity that is closely related to the total breeding ratio (TBR) in the test assembly. A novel methodology developed during the collaboration was applied to arrive at estimates to design safety factors that fusion blanket designers can use to ensure that the achievable TBR in a blanket does not fall below a minimum required value. Associated with each safety factor is a confidence level, designers may choose to have, that calculated TPR will not exceed the actual measured value. Higher confidence levels require larger safety factors. Tabular and graphical forms for these factors are given, as derived independently for TPR from Li-6 (T_6), Li-7 (T_7), and natural lithium (T_n). Furthermore, distinction was made between safety factors based on the technique applied, discrete ordinates methods, and Monte Carlo methods in the U.S. calculations, JAERI's calculations, and in both calculations considered simultaneously. The derived factors are applicable to TPR in Li_2O breeding material; nevertheless, the results can be used as initial guidance to assist in resolving the tritium self-sufficiency issue in other breeding media.

I. INTRODUCTION

Verification of the anticipated performance of the major fusion reactor components prior to construction through integral experiments is an integrated part of the design process. This is required to provide enough experimental databases for approval and licensing purposes, on one hand, and to verify the prediction capability and generation of design safety factors, on the other. Generally, the neutronics research and development (R&D) issues cover several areas including but not limited to the tritium production rate (TPR) in a breeding media, induced activation and decay heat, nuclear heating, bulk and biological shield, and radiation streaming through open paths. One of the prime goals for utilizing fusion energy is to sustain self-sufficiency in tritium in reactors based on the deuterium-tritium (D-T) fuel cycle.[1-3] Failure to meet certain accuracy requirements in TPR prediction is therefore a critical issue that could rule out some blanket concepts. To resolve this particular issue, many fusion integral experiments[4-33] on tritium breeding measurements and analysis were performed during the last decade within the U.S. Department of Energy (U.S. DOE)/Japan Atomic Energy Research Institute (JAERI) collaboration on fusion blanket neutronics with the objective of quantifying the overall uncertainties in TPR prediction with current calculational tools and databases. The experiments utilized the 14-MeV neutron source located at the Fusion Neutronics Source (FNS) facility at JAERI. Local TPR throughout a Li_2O test assembly was measured, among other reactions, under varying operational and geometrical conditions. Among the conditions varied are the following: a 14-MeV point source versus a simulated line source, open geometry versus closed geometry, etc. The parameter used for code and data verification is the ratio of calculated-to-experimental value, c/e.

The objective of this paper is to evaluate the overall prediction uncertainty in TPR from Li-6 (T_6), Li-7 (T_7), and natural lithium (T_n). The experimental and calculational data sets of local TPR in each experiment, i, were propagated to give estimate to the prediction uncertainty, u_i, of the line-integrated TPR and its standard deviation, σ_i. The line-integrated TPR was chosen as the response since it is closely related to the total breeding ratio (TBR) in the test assembly. An approach was also pursued to give estimates to the prediction uncertainty in the volume-integrated TPR based on measurements and calculations of local TPR in the traverse direction. The methodology discussed in Part I of this paper[3] was applied to arrive at estimates to design safety factors that fusion blanket designers can use to ensure that the achievable TBR in a blanket does not fall below a minimum required value (see Ref. 1). These correction/safety factors were determined and compared under several conditions including the calculational method and database used, the measuring technique applied, and source and geometrical conditions of the test assembly.

In Sec. II, the experiments performed during the collaborative program and the experimental techniques used to measure TPR are briefly described with emphasis on the difference in the geometrical arrangements among these experiments. Brief discussion on the calculational methods used is given in Sec. III. Section IV is devoted to describing the calculational procedures followed to estimate the prediction uncertainty in the line-integrated TPR, u_i's, and their associated standard deviations, σ_i's. Procedures to estimate similar parameters are also given in Sec. IV for the volume-integrated TPR. Section V gives the normalized density functions (NDFs) constructed from the parameters u_i's and σ_i's, and used to derive safety factors (in graphical and tabular form) for the line-integrated T_6, T_7, and T_n. The conclusions of this work are cited in Sec. VI.

II. THE EXPERIMENTS

II.A. Description

Phase I experiments, started in October 1984 and completed in March 1986, are characterized by being performed in an open geometry with a 14-MeV point source. The test assembly is a cylinder of diameter D = 60 cm and length L = 61 cm constructed from Li_2O blocks of different sizes; most of them are of the dimensions 5.08 cm × 5.08 cm × 5.08 cm. The test assembly is loaded in the experimental cavity connecting target room 2 (4.96-m × 4.96-m × 4.5-m height), where the experiments were performed, and the large target room 1. The physical center of the rotating target (neutron source generator for the 14.1-MeV neutrons) is at a distance of ~2.48 m from the side walls and at 2.7 m and 1.8 m from the ceiling and the floor level, respectively. Three categories of experiments were conducted:

1. The reference experiment (P1-REF), the test assembly consisted of a single Li_2O material.

2. The first wall experiments, a 0.5-cm-thick stainless steel first wall (316SS) was placed in front of the Li_2O assembly; then a 0.5-cm-thick polyethylene (PE) plate was placed between the first wall and the assembly. This sequence of experiments was repeated, but a 1.5-cm-thick first wall was deployed instead, as shown in Fig. 1a. This series of experiments is designated by (P1-WFW).

3. The beryllium experiments, three configurations were assembled, i.e., 5-cm-thick Be, 10-cm-thick Be, and 5-cm-thick + 5-cm-thick Be layers were placed in front of the Li_2O assembly, separately, as shown in Fig. 1b. This series of experiments is designated by (P1-WBE). Details of the measurements and analysis performed in this phase can be found in Refs. 4, 5, and 6.

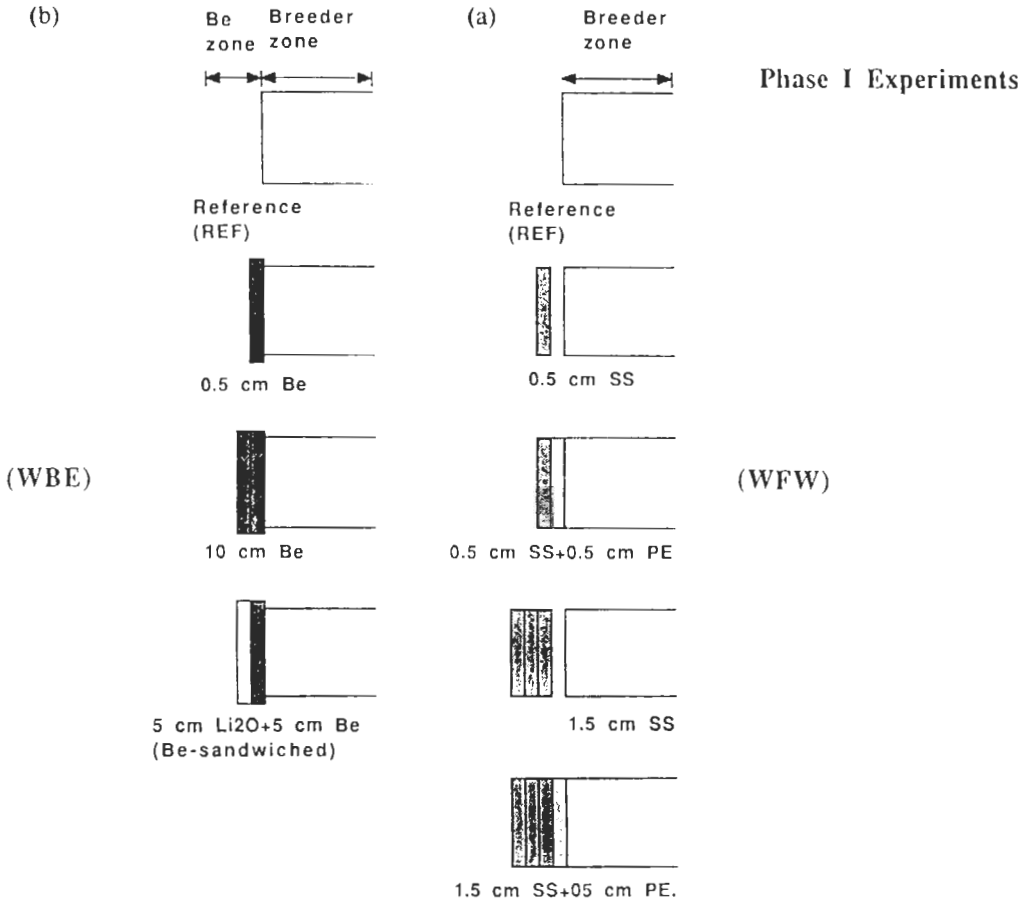

Fig. 1. Arrangements for (a) the first wall experiments (WFW) and (b) the beryllium experiments (WBE) of Phase I.

Phase II experiments were also performed in target room 2 with a point source. The test assembly is a rectangular shape of dimensions 86.4 cm × 86.4 cm × 60.71 cm and was placed at one end of a rectangular enclosure made of Li_2CO_3, and the D-T neutron source was placed inside the cavity at a distance ~78 cm from the square front surface of the test assembly as shown in Fig. 2. The dimensions of the inner cavity were 87 cm × 87 cm × 124 cm, and the thickness of the Li_2CO_3 enclosure was 20.5 cm. A 5-cm-thick PE layer was included at the outer surface of the enclosure in order to eliminate the low-energy, room-returned component of the neutrons reflected by the room walls and reentering the test zone.

Three experiments were performed in Phase IIA. The first is the reference (P2A-REF) experiment where only the Li_2O material constituted the test assembly. In the second experiment, designated by (P2A-BEF), the first 5 cm at the front were replaced by beryllium. A 5-cm-thick Be layer was sandwiched between a 5-cm-thick Li_2O front layer and the rest of the Li_2O test zone in the third experiment, designated (P2A-BES), as shown in Fig. 2a. The experiments performed in Phase IIB were similar except that the inner surface of the Li_2CO_3 enclosure was covered by a 5-cm-thick Be layer in addition to a 0.5-cm-thick SUS-304 first wall as shown in Fig. 2b. Three experiments were performed: The reference (P2B-REF) experiment had no Be layer in front of the Li_2O test zone; the beryllium front (P2B-BEF) experiment (0.5-cm-thick Be layer preceded the Li_2O test assembly) was without a first wall, and the Be front experiment was with a first wall (P2B-BEFWFW) of 0.5-cm thickness. Details of the measurements and analysis for Phases IIA and IIB can be found in Refs. 7 through 15.

Two experiments were performed in Phase IIC that focused on the heterogeneity effects on tritium production and other reaction rate profiles, namely,

1. The water coolant channel (P2C-WCC) experiment: In this experiment simulated water coolant channels were introduced in the assembly with the dimensions shown in Fig. 3a. One coolant channel was placed behind a 5-mm-thick first wall that preceded the Li_2O test assembly (~60 cm thick) and two other channels were placed at a depth of 10 cm and 20 cm, respectively, and three drawers were utilized as shown in Fig. 3a.

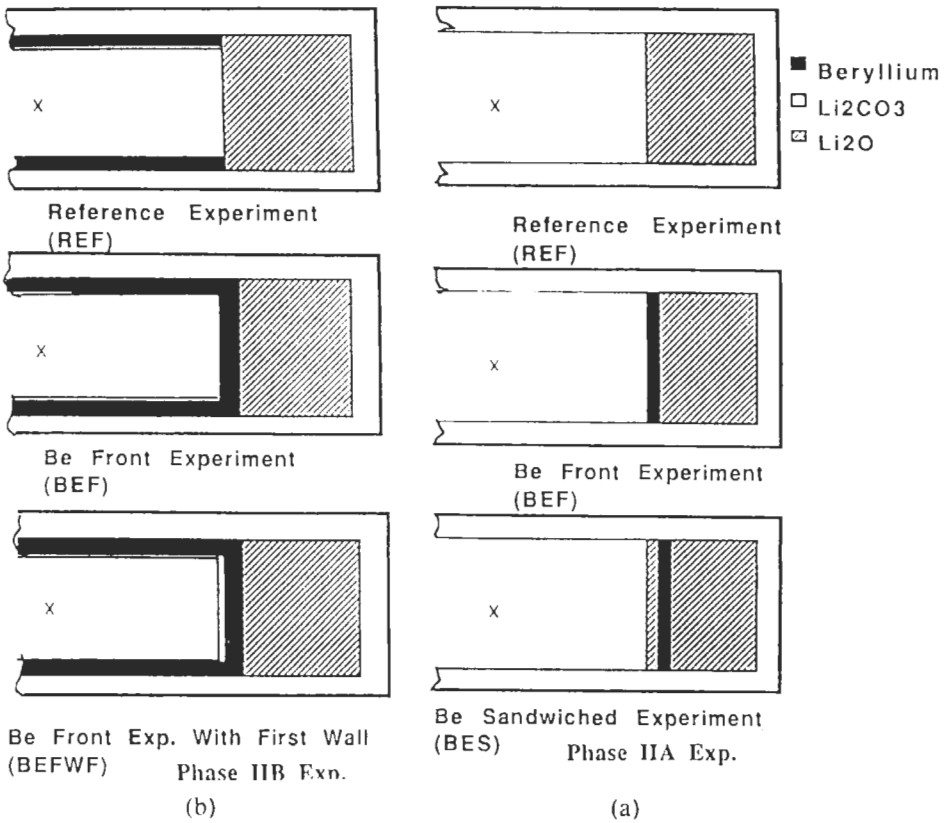

Fig. 2. Arrangements for (a) Phase IIA experiments (b) Phase IIB experiments.

2. The multilayer beryllium edge-on experiment (P2C-BEO) in which multiple layers of Li_2O and beryllium were arranged in an edge-on, horizontally alternating configuration for a front depth of 30 cm followed by the Li_2O breeding zone and three drawers were also utilized, as shown in Fig. 3b. More details on this phase can be found in Refs. 16 through 22.

In Phase IIIA, the geometrical arrangement and source conditions were different from previous phases. An annular test assembly of 204-cm length and outer dimensions of 130.1 cm × 130.1 cm with inner square cavity dimensions of 42.55 cm × 42.55 cm was moved periodically back and forth relative to a stationary point source, and hence, a simulated line source was created at the central axis of the cavity. The test assembly consisted of a 1.5-cm-thick Type 304 stainless steel first wall followed by a 20-cm-thick Li_2O zone and a 20-cm-thick Li_2CO_3 zone, as shown in Fig 4. The outer surface was covered by a 1.6-cm PE layer, and both ends of the assembly were left open. The length of the simulated line source was 200 cm. Three radial drawers were installed through which measurements were taken: namely drawer A (its center at axial distance $z = -53.4$ cm, ends of assembly at $z = \pm 102$ cm), drawer B ($z = -2.53$ cm), and drawer C ($z = 48.35$ cm). In Phase IIIB, a 2.54-cm-thick carbon layer was added at the inner surface of the cavity to act as an armor zone found in fusion reactors. In Phase IIIC, a squared opening of 376 × 425.5 mm was made at the center of the Phase IIIB system whose cavity is lined by graphite. Measurements of TPR were made at the three drawers (A, B, and C) facing the large opening and along a radial drawer D adjacent to the opening itself. More details on Phase III experiments can be found in Refs. 23 through 31. Table I summarizes all the experiments considered in this study. In some of these experiments, the prediction uncertainty in TPR was calculated separately in several subzones inside the breeding zone. For example, in the beryllium sandwiched experiment of Phase IIA (P2A-BES), two subzones were considered (zone 1 in front of the Be layer and zone 2 behind it). Five subzones (zone 1 to zone 5) were considered in the water coolant channel experiment of Phase IIC (P2C-WCC) whose boundaries are described in Ref. 21. Additionally, in the experiment (case) labeled P3A-All, the experimental and the calculational data sets in the three drawers A, B, and C were combined together to give an overall profile of the TPR averaged over the three drawers.

II.B. Measuring Methods

Several techniques were used to measure the local tritium production rate from Li-6 (T_6). These are the

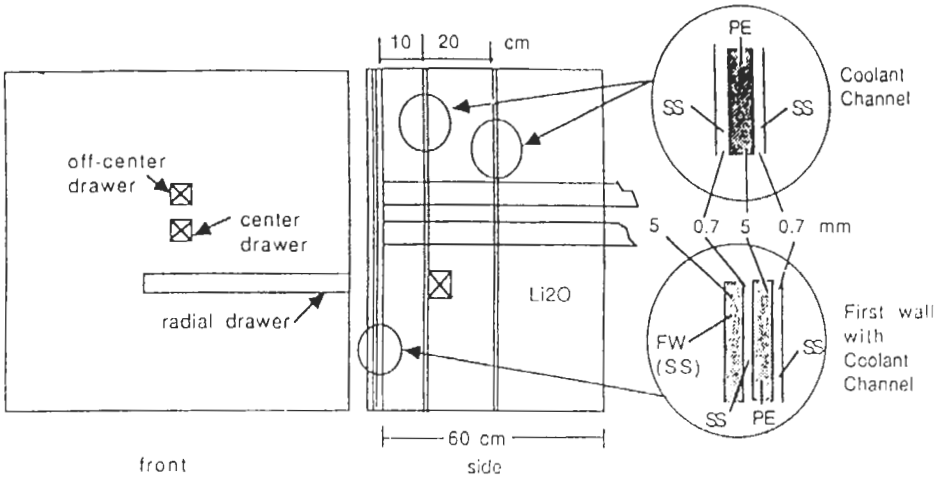

(a)

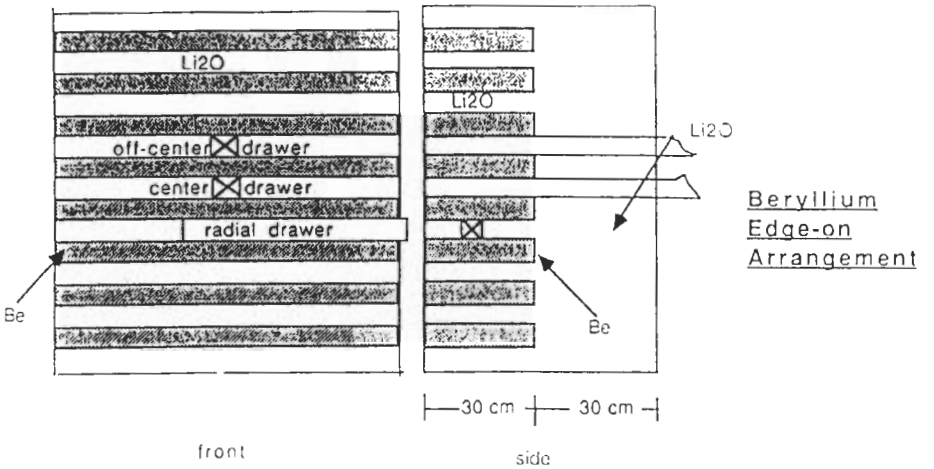

(b)

Fig. 3. The test assembly used in the Phase IIC experiments: (a) water coolant channels (WCC) arrangement, and (b) beryllium edge-on arrangement (BEO).

Li-glass on-line method,[34] the Li-metal method, and the Li_2O pellet method. Tritium production rates from Li-7 (T_7) were measured indirectly by the NE213 detector[35] and by Li-metal and Li_2O pellet detectors. The TPR from natural lithium (T_n) was measured by the Li_2O pellet and the composed method. In the later, the TPR from Li-6 measured by the Li-glass detector and the TPR from Li-7 measured by the NE213 method at a particular spatial location were combined (using the natural enrichment value of Li-6, $a_6 = 0.0742$) to arrive at an experimental value for T_n. In addition zonal technique was used to measure T_6, T_7, and T_n using the liquid scintillation method. The measurements with this technique were performed on the Li_2O blocks along the central axis of the assembly whose dimensions are ~5 cm × 5 cm × 5 cm. Details of these measuring techniques can be found in Refs. 15, 17, and 18.

III. CALCULATIONAL METHODS

Both the deterministic [discrete ordinates (DO)] and the Monte Carlo (MC) methods were used in analyzing the experiments except for the BEO and Phase IIIC experiments which called for three-dimensional treatment by the Monte Carlo method. In the U.S. calculations, the MCNP code,[36] version 3A, was used in analyzing Phase I and IIA experiments while version 3B was applied in analyzing subsequent experiments. The pointwise continuous energy/angle cross-section library RMCCS/BMCCS, which is based on ENDF/B-V, version 2, was used in the Monte Carlo analysis. The DOT4.3 (Ref. 37) and DOT5.1 codes were used in the two-dimensional Sn treatment. The first collision code RUFF (Ref. 38) was used to generate the uncollided fluxes needed for the DOT calculations. The MATXS6

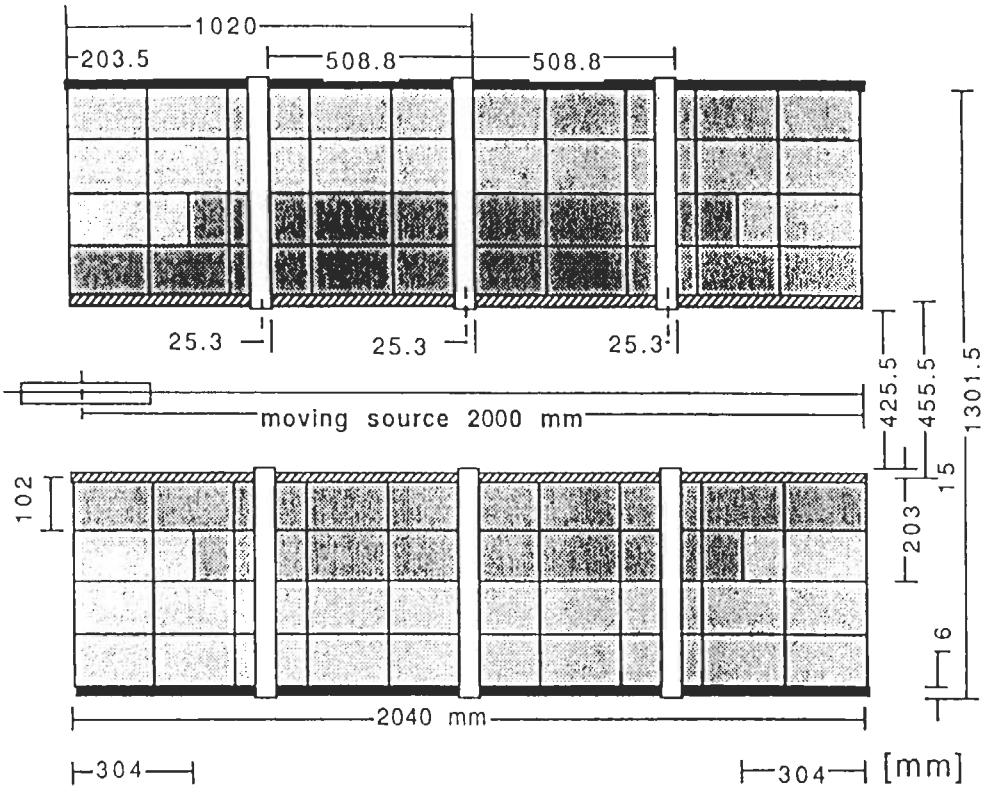

(a) Elevation View

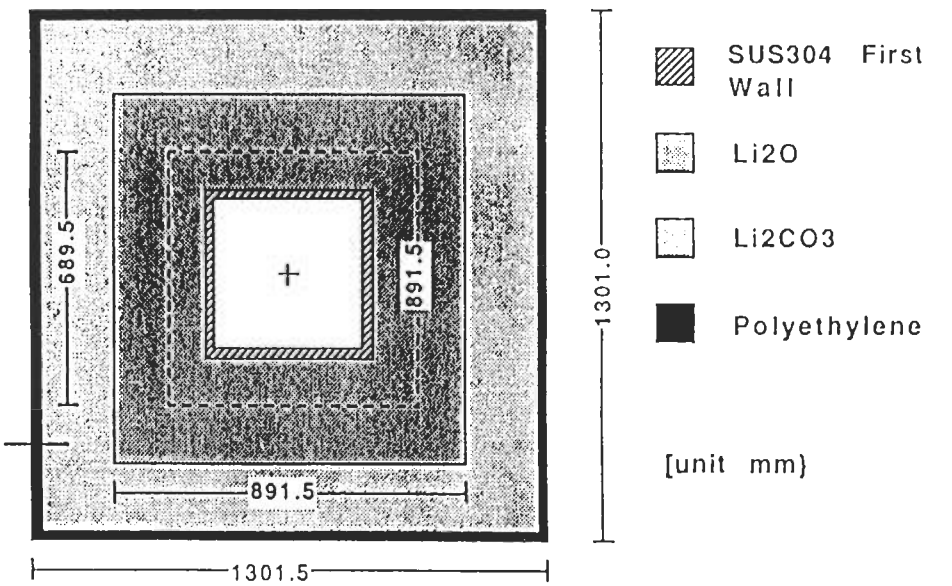

(b) Cross-Sectional View

Fig. 4. Geometrical arrangement for Phase IIIA (simulated line source) experiment.

library[39] [80-group neutrons] was used in the DOT calculations with P5-S16 approximation, while the MATXS5 (Ref. 39) [30-group neutrons] was applied (P3-S16) in Phase III analysis. The beryllium data of LANL (Ref. 40) was used in the U.S. analysis.

The MORSE-DD (Ref. 41) code was used by JAERI in the MC calculations, and it utilizes the double differential cross-section library DDL/J3P1 (125 neutron group) based on the JENDL3/PR1 data file. In some cases, the GMVP code[42] was also used to

TABLE I

Abbreviation for the Experiments Conducted in Phases I, II, and III

Phase	Experiment/Case	Abbreviation
I	Reference Experiment	P1-REF
I	First Wall Experiment-FW = 0.5 cm	P1-WFW (0.5)
I	First Wall Experiment-FW = 1.5 cm	P1-WFW (1.5)
I	Beryllium Experiment-Be = 5 cm	P1-WBE (5 cm)
I	Beryllium Experiment-Be = 10 cm	P1-WBE (10 cm)
IIA	Reference Experiment	P2A-REF
IIA	Beryllium Front Experiment	P2A-BEF
IIA	Beryllium-Sandwiched Experiment	P2ABES
IIB	Reference Experiment	P2B-REF
IIB	Beryllium Front Experiment	P2B-BEF
IIB	Beryllium Front with First Wall Expt.	P2B-FEFWFW
IIC	Water Coolant Channel Experiment	P2C-WCC
IIC	Beryllium Edge-On Experiment	P2C-BEO
IIIA	Reference Experiment-Drawer A	P3A-DA
IIIA	Reference Experiment-Drawer B	P3A-DB
IIIA	Reference Experiment-Drawer C	P3A-DC
IIIA	Reference Experiment-Drawer A&B&C	P3A-All
IIIB	Armore Experiment-Drawer A	P3B-DA
IIIB	Armore Experiment-Drawer B	P3B-DB
IIIB	Armore Experiment-Drawer C	P3B-DC
IIIB	Armore Experiment-Drawer A&B&C	P3B-All
IIIC	Large Opening Experiment-Drawer A	P3C-DA
IIIC	Large Opening Experiment-Drawer B	P3C-DB
IIIC	Large Opening Experiment-Drawer C	P3C-DC
IIIC	Large Opening Experiment-Drawer D	P3C-DD
IIIC	Large Opening Expt.-Drawer A&B&C	P3C-All

reanalyze some experiments, particularly in Phase III with JENDL3 data. The FSXJP7 library (P_7, 125-g) was used in JAERI's calculations with DOT3.5/GRTUNCL codes[43] and is based on JENDL3/PR2. In folding the NE213 experimental data to obtain measured values for T_7, the JENDL3/PR2 data for the ^{7}Li(n,n′α)t cross section was used.

IV. THEORY

IV.A. The Prediction Uncertainty in the Line-Integrated TPR

Using the calculation data set, $\{z_i, c_i, \sigma_{ci}^2\}$, where z_i's are the measuring locations at the central axis of the test assembly, c_i's are the calculational data at locations z_i's, and σ_{ci}^2's are their associated variances, one finds the curve that can best fit the data c_i's using the least-squares fitting method.[44,45] This can be undertaken by finding a model to fit N′ data points (z_i, c_i), i = 1,..., N′ which has M adjustable parameters (coefficients), a_{ci}, i = 1,...,M, such that the quantity

$$\chi^2 = \sum_{i=1}^{N'} \left[\frac{c_i - f(z_i, a_{c1}, \ldots, a_{cM})}{\sigma_{ci}} \right]^2 \qquad (1)$$

is minimal. If "f" is a linear combination of specified functions of z, i.e., $Z_k(z)$, then

$$f(z) = \sum_{k=1}^{M} a_{ck} \cdot Z_k(z) \qquad (2)$$

and when χ^2 is minimized, this leads to the normal equations[44]

$$0 = \sum_{i=1}^{N'} \frac{1}{\sigma_{ci}^2} \left[c_i - \sum_{k=1}^{M} a_{ck} \cdot Z_k(z) \right] Z_k(z_i) \; . \qquad (3)$$

These equations are solved using the singular decomposition matrix approach[44] to yield the fitting coefficients, a_{ck}, k = 1,...,M, and their covariance matrix, $COV(a_{ck}, a_{ck'})$, which depends on the standard deviations, σ_{ck}, at the measuring points z_i, i = 1,...,N′. In performing the line integration, two options could be adopted. The fitting equation could be one of the following forms:

$$f(z) = \sum_{k=1}^{M} a_{ck} \cdot z^{k-1} \qquad \text{(polynomials)} \qquad (4)$$

$$f(z) = a_{c1} \cdot \exp\left(\sum_{k=2}^{M} a_{ck} \cdot z^{k-1} \right) \qquad \text{(exponential)} \; . \qquad (5)$$

The second form is used when the fitted values vary steeply with distance z (e.g., T_6 near boundaries). In the case of the polynomial form, the integration, C, over a distance between Z_1 and Z_2 is given by

$$C = \sum_{k=1}^{M} a_{ck} \cdot \int_{Z_1}^{Z_2} z^{k-1}\, dz \tag{6}$$

and the variance of C, σ_C^2, is given by

$$\sigma_C^2 = \sum_{k=1}^{M} \sum_{k'=1}^{M} f_k\, COV(a_{ck}, a_{ck'}) f_{k'} \ , \tag{7}$$

where

$$f_k = \int_{Z_1}^{Z_2} z^{k-1}\, dz \ . \tag{8}$$

In the case of the exponential form, we have

$$\ln f = F = \sum_{k=1}^{M} a'_{ck} z^{k-1}$$

$$C = \int_{Z_1}^{Z_2} f\, dz = \int_{Z_1}^{Z_2} e^F\, dz \tag{9}$$

and the variance of C, σ_C^2, is given by

$$\sigma_C^2 = \sum_{k=1}^{M} \sum_{k'=1}^{M} f'_k\, COV(a'_{ck}, a'_{ck'}) f'_{k'} \tag{10}$$

where

$$f'_k = \int_{Z_1}^{Z_2} f z^{k-1}\, dz \ . \tag{11}$$

Likewise, using the experimental data set, $\{z_i, e_i, \sigma_{ei}^2\}$, we perform the above procedures to obtain the fitting coefficients a_{ek}'s, the covariance matrix $COV(a_{ek}, a_{ek'})$, the integrated value E, and its variance σ_E^2. The prediction uncertainty in the integrated TPR is quantified in terms of the quantity, u, where $u = (C/E - 1)$. The relative variance in u, σ_r^2, is the algebraic sum of σ_{Cr}^2 and σ_{Er}^2; i.e., the relative variance in the integrated values C and E, given by $\sigma_{Cr}^2 = \sigma_C^2/C^2$ and $\sigma_{Er}^2 = \sigma_E^2/E^2$, respectively. No correlation has been assumed between the integrated quantities C and E.

IV.B. The Prediction Uncertainty in the Volume-Integrated TPR

In Phase II, the test assembly is assumed to be a cylinder. Measurements for TPR were made along two radial drawers in addition to axial measurements. To quantify an estimate to the prediction uncertainty in the volume-integrated TPR and its variance, the following is applied to the experimental and calculational data sets, $\{z_i, e_i, \sigma_{ei}^2\}$ and $\{z_i, c_i, \sigma_{ci}^2\}$. We first perform curve fitting to the data points $\{z_i, f_i, \sigma_{fi}^2\}$ ($f \equiv c$ or e) on the z axis of the test assembly and get the fitting coefficients a_k, $k = 1, \ldots, M$, and the covariance matrix $COV(a_k, a_{k'})$. Using the polynomial expansion case we have

$$y_0(r = 0, z) = \sum_{k=1}^{M} a_k z^{k-1} \ . \tag{12}$$

Next, we assume that the TPR at any location in the test assembly has the following r and z dependence

$$y(r,z) = \phi(r) \cdot y_0(r = 0, z) \ , \tag{13}$$

where for a given $z = z_l$, $\phi(r)$ is the ratio of the function at r to the corresponding function at $r = 0$. This implies that the relative variation in r direction with respect to the axial values at $r = 0$ is assumed the same for all values of z. The function $\phi(r)$ could be expressed in polynomial form as

$$\epsilon(r) = \phi(r) - 1 = \sum_{j=1}^{J} c_j r^j \ . \tag{14}$$

For a given $z = z_l$ (e.g., a radial drawer at $z = z_l$), curve fitting for the function $\epsilon(r)$ is performed using the data points, $\epsilon^{data}(r_i)$, obtained from the relation

$$\epsilon^{data}(r_i) = [y^{data}(r_i, z_l)/y_0(r = 0, z_l)] - 1 \ , \tag{15}$$

where the relative standard deviation, $\sigma^2_{\epsilon data}(rel)$, at the data points $\epsilon^{data}(r_i)$ are obtained from the relation

$$\sigma^2_{\epsilon data}(rel) = \sigma^2_{\phi data}(rel) = \sigma^2_{y data}(rel) + \sigma^2_{y_0}(rel) \ , \tag{16}$$

where $\sigma^2_{y data}(rel)$ is obtained from the measured (or calculated) data (i.e., is known) and

$$\sigma^2_{y_0}(rel) = \left(\frac{1}{y_0}\right)^2 \cdot \sum_{k=1}^{M} \sum_{k'=1}^{M} z_l^{k-1}\, COV(a_k, a_{k'}) z_l^{k'-1} \ . \tag{17}$$

Now we can obtain from curve fitting in r direction the coefficients b_j's and covariance matrix $COV(c_j, c_{j'})$ using the data set $\{r_i, \epsilon^{data}, \sigma^2_{\epsilon data}\}$. The volume-integrated quantity, I, is given by

$$I = 2\pi \int_0^r r \cdot \phi(r)\, dr \int_{Z_1}^{Z_2} y_0(z)\, dz = 2\pi I_\phi I_{y_0} \tag{18}$$

and the variance of this integrated quantity is given by

$$\sigma_I^2(rel) = \sigma^2_{I_{y_0}}(rel) + \sigma^2_{I_\phi}(rel) \ , \tag{19}$$

where $\sigma^2_{I_{y_0}}(rel) = \sigma^2_{I_{y_0}}/I^2_{y_0}$,

$$\sigma^2_{I_{y_0}} = \sum_{k=1}^{M} \sum_{k'=1}^{M} f_k\, COV(a'_k, a'_{k'}) f_{k'} \ , \tag{20}$$

$$f_k = \int_{Z_1}^{Z_2} z^{k-1}\, dz \ , \quad \sigma^2_{I_\phi}(rel) = \sigma^2_{I_\phi}/I^2_\phi \ , \tag{21}$$

$$\sigma^2_{I_\phi} = \sum_j \sum_{j'} F^j_\phi\, COV(c_j, c_{j'}) F^{j'}_\phi \ , \tag{22}$$

and

$$F^j_\phi = 2\pi \int_0^R r^{j+1}\, dr \ . \tag{23}$$

When applying the above procedures to the calculational and experimental data sets, we now have the quantities, $I_c = C$, σ^2_{Cr}, $I_e = E$, and σ^2_{Er}. The prediction uncertainty in the volume-integrated TPR is $u = (C/E - 1)$, which has relative variance, σ_r^2, given by the algebraic sum of σ^2_{Cr} and σ^2_{Er}.

IV.C. The Prediction Uncertainty in TPR from Natural Lithium (T_n) as Obtained from the Prediction Uncertainty in the Line-Integrated T_6 and T_7

In a given experiment, the prediction uncertainty in T_n, u_n ($= C_n/E_n - 1$), can be obtained from the prediction uncertainty in the line-integrated T_6, u_6, measured by the Li-glass method and from the prediction uncertainty in the line-integrated T_7, u_7, measured by the NE213 method. The governing expressions in this case are

$$C_n = \alpha_6 C_6 + \alpha_7 C_7 \ , \qquad E_n = \alpha_6 E_6 + \alpha_7 E_7 \qquad (24)$$

$$\sigma^2_{C_n} = \alpha_6^2 \sigma^2_{C_6} + \alpha_7^2 \sigma^2_{C_7} \ , \quad \sigma^2_{E_n} = \alpha_6^2 \sigma^2_{E_6} + \alpha_7^2 \sigma^2_{E_7} \qquad (25)$$

$$\sigma^2_{nr} = \sigma^2_{C_{nr}} + \sigma^2_{E_{nr}} \qquad (26)$$

$$\sigma^2_{C_{nr}} = \sigma^2_{C_n}/C_n^2 \ , \qquad \sigma^2_{E_{nr}} = \sigma^2_{E_n}/E_n^2 \ , \qquad (27)$$

where α_6 and α_7 are the enrichment of Li-6 (0.0742) and Li-7 (0.9258) in natural lithium and $\sigma^2_{C_6}$ and $\sigma^2_{C_7}$ are the variance in the integrated values C_6 and C_7. Likewise, the variance in the integrated values E_6 and E_7 are $\sigma^2_{E_6}$ and $\sigma^2_{E_7}$. The quantity σ^2_{nr} is the relative variance of the calculated-to-experimental value, C_n/E_n.

V. RESULTS AND DISCUSSION

The prediction uncertainty in the line-integrated T_6 and T_7 [$u_i = (C_i/E_i - 1) \times 100$] in each experiment, i, based on the DO and MC calculations along with the associated standard deviations, $\pm\sigma_i$'s, were obtained according to Eqs. (1) through (11). The calculational uncertainties in the Monte Carlo calculations are those arising from the statistical treatment. In the discrete ordinates case, the deviations σ_i's include the experimental errors only. No account was made in the calculational errors to the contribution arising from nuclear data uncertainties. Estimates to uncertainties in TPR due to nuclear data uncertainties can be found elsewhere.[46-48] Furthermore, some of the experimental errors were not readily available at some locations in some of the experiments. In these cases, the following experimental errors were assumed:

NE213 measurements	~6.5%
Li-glass, Li-metal, Li_2O pellet Measurements for T_6 and T_7	~3.5%
Zonal TPR for T_6, T_7	~3.5%.

Unlike other phases, the experimental errors of the Li_2O pellet in Phase III were large ($\geq$~10%).

V.A. Volume- Versus Line-Integrated TPR

The prediction uncertainties in the volume-integrated TPR in the reference experiment of Phase I (P1-REF) were calculated according to Eqs. (14) through (23), and the results were compared to those obtained for the line-integrated TPR. As shown below, the prediction uncertainties, u_i, are within a few percent for the integrated quantities of T_6 and T_7. This demonstrated the validity of the assumptions and procedures discussed in Sec. IV.B. Furthermore, the design safety factors derived for the line-integrated TPR could be used as reasonable indices for the design safety factors of TBR.

Reference System of Phase I	Transport Code	Prediction Uncertainty in TPR: Line-Integrated (%)	Prediction Uncertainty in TPR: Volume-Integrated (%)
TPR from Li-6 (T_6)	DOT4.3	11.5	10.1
	MCNP	5.1	5.0
TPR from Li-7 (T_7)	DOT4.3	19.4	20.1
	MCNP	9.2	7.5

V.B. The Prediction Uncertainties in the Line-Integrated TPR from Li-6 (T_6)

V.B.1. Li-Glass Measuring Technique

The prediction uncertainty in the line-integrated T_6 as obtained by the U.S. are shown in Fig. 5 based on the Li-glass measurements. The counterpart uncertainties based on JAERI's calculations are shown in Fig. 6. Figure 7 shows the histogram of NDF of the prediction uncertainty, u, based on all the discrete ordinates and Monte Carlo cases of the U.S. shown in Fig. 5 and was calculated according to the methodology described in Ref. 3. Also shown is the NDF in the case where the experimental errors are ignored while accounting only for the calculational errors. The contribution to σ_i's that comes only from the calculational errors is represented by the black bars shown in Figs. 5 and 6 and in subsequent figures. The Gaussian curves that have the same mean prediction uncertainty, $\bar{u}$, and standard deviation, σ_u, [see Eqs. (4) and (7) in Ref. 3] as those of the NDFs are also shown in Fig. 7 for comparison. The Gaussian curves have close representation of the NDFs, particularly in the case when the calculational and experimental (C&E) errors are included in the analysis. Without considering the experimental errors, there are more distinctive dips in the NDF, which is expected since the error bars shown in Fig. 5 are shorter in this case and less overlapping takes place between the possible prediction uncertainties among all the experiments (cases) considered.

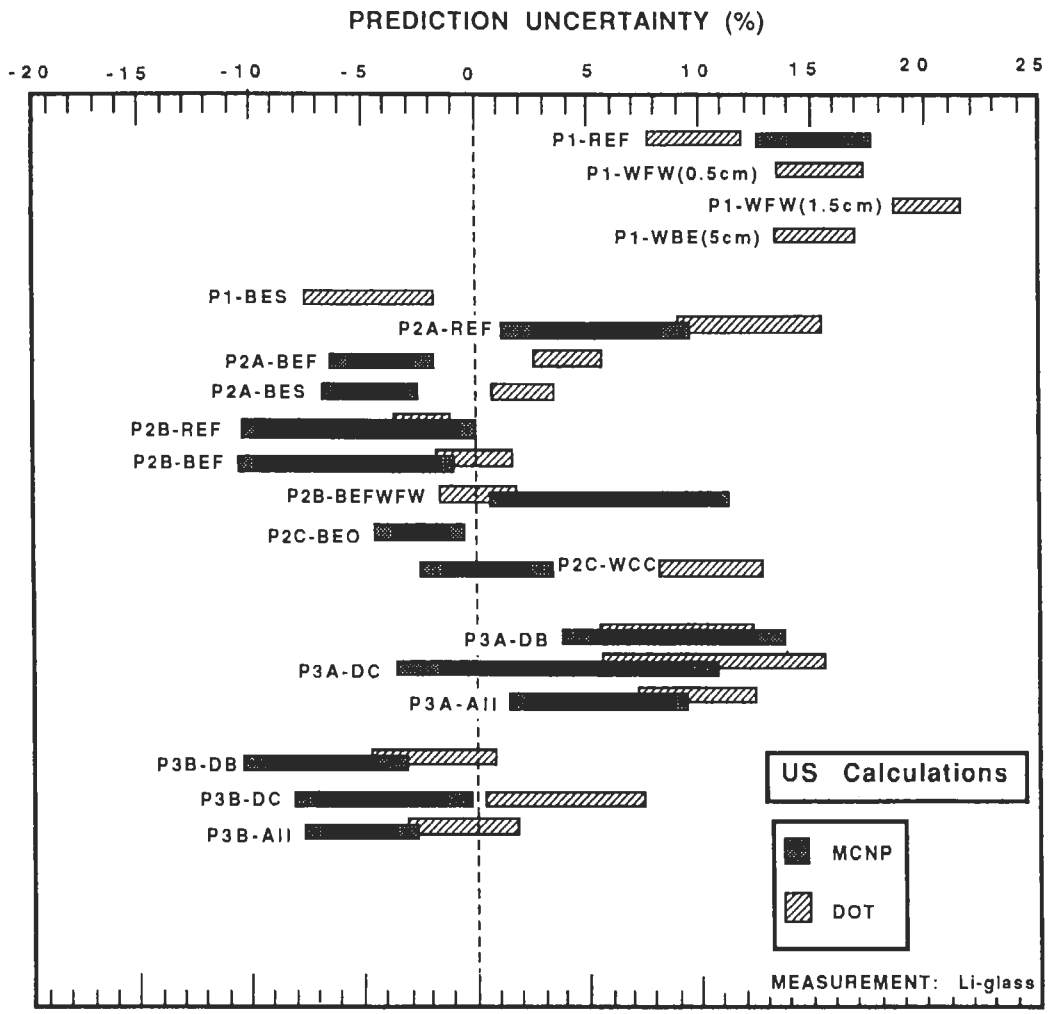

Fig. 5. The prediction uncertainty in the line-integrated TPR from Li-6 (T_6) (U.S. calculations, Li-glass measurements).

The NDF based on JAERI's cases given in Fig. 6 is depicted in Fig. 8. Comparing the Gaussian curves that approximate the NDFs, the mean prediction uncertainty, $\bar{u}$, is lower than the one obtained by the U.S. by ~3%. In addition, larger dips and peaks are found in the NDF when only the C errors are considered than those seen in Fig. 7 due to the fact that the statistical errors in the Monte Carlo calculations of JAERI are generally smaller than in the U.S. case, leading to lesser overlapping among the uncertainty bars shown in Fig. 6. Figure 9 shows the NDF for the prediction uncertainty u constructed from all the cases shown in Figs. 5 and 6. Clearly in this case the NDFs are smoother than the ones based only on the U.S. or JAERI calculations, and their shape is closer to Gaussian.

The relationship between the accepted (adopted) safety factor S_k [$= (u_k/100) + 1 = C/E$] and the associated confidence level, $(CL)_k$, in percentage, is shown in Fig. 10 when the C&E errors are included (see Ref. 3). The labels U.S., JAERI, and U.S.&JAERI denote that the curves are obtained from the NDFs given in Figs. 7, 8, and 9, respectively. If no safety factor is used ($S_k = 1 = C/E$), the confidence level that calculated T_6 will not exceed the actual measured value is ~42% in the U.S. case and ~46% in JAERI's case. To have a 100% confidence, the safety factor to be used is 1.28 in the U.S. case and 1.18 in JAERI's case. (Statistically, no such a 100% confidence can be achieved since there are uncertainties in the curves shown in Figs. 7, 8, and 9 themselves due to the limited number of cases considered, n, whose magnitude are $\sim 1/n^{1/2}$. The factors 1.28 and 1.18 can be viewed as the largest values of C/E as evidenced from the analysis of all experiments, considering both the experimental and calculational errors. They can also be viewed as the most conservative correction/safety factors.) Thus, for the same confidence level, the required safety factors are larger in the U.S. case than in the JAERI case. Their values, however, approximately assume the average between the two cases when the

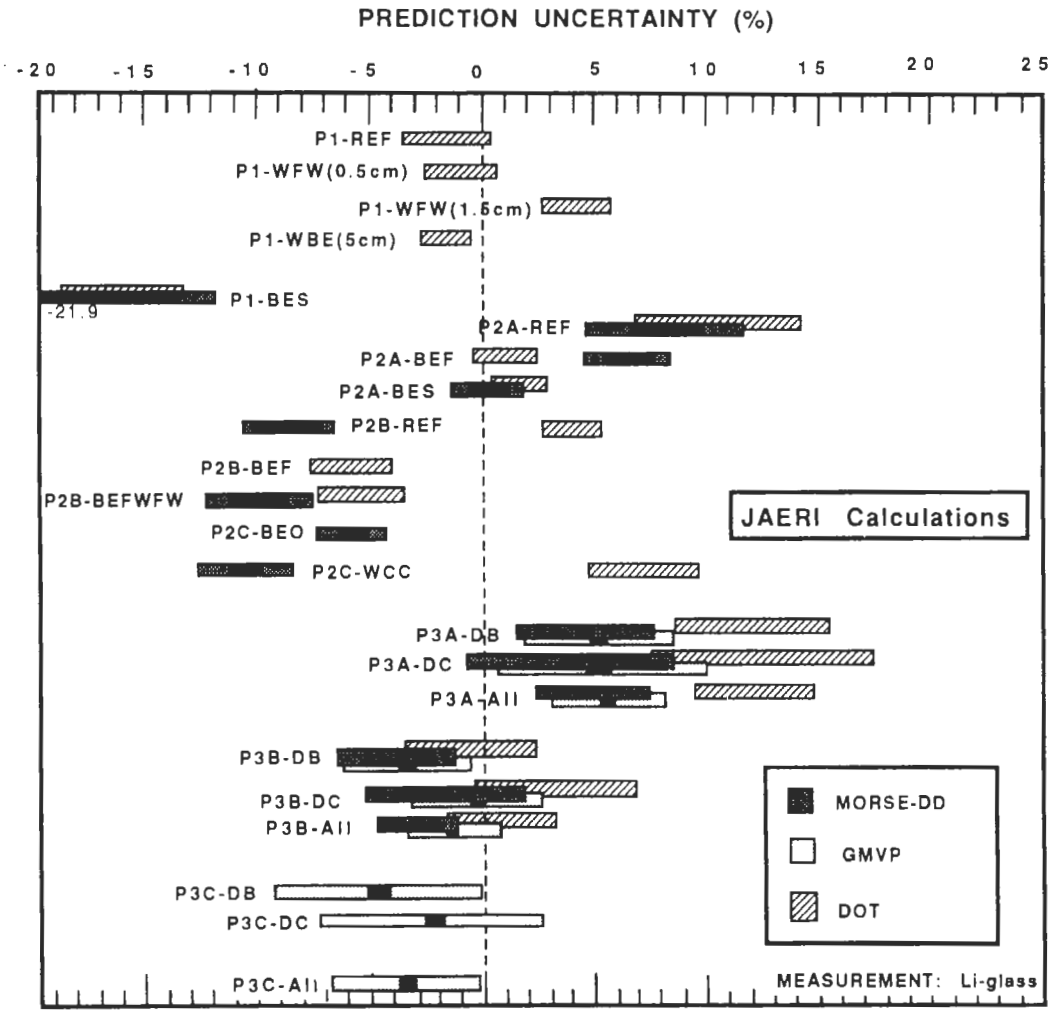

Fig. 6. The prediction uncertainty in the line-integrated TPR from Li-6 (T_6) (JAERI's calculations, Li-glass measurements).

NDF constructed from all cases shown in Figs. 5 and 6 is used to derive the $(CL)_k - S_k$ curve. In this later case, the most conservative safety factor is the largest factor obtained from the U.S. and the JAERI cases when treated separately (i.e., $S_k \sim 1.28$). The $(CL)_k - S_k$ curves when only the C errors are considered are shown in Fig. 11. The above observations still hold in this case. For the same confidence level, the required safety factors are smaller than those shown in Fig. 10. At $(CL)_k = 100\%$, $S_k = 1.24$ and 1.14 in the U.S. and JAERI cases, respectively, and are lower than the corresponding ones ($S_k = 1.28$ and 1.18) shown in Fig. 10 by ~3%; a value which is comparable to the experimental errors of the Li-glass measurements. Note that the NDFs shown in Figs. 7, 8, and 9 are based on $\Delta u_j = 2\%$. It was shown in Ref. 3 that using a wider interval width leads to more conservative estimates to the design safety factors. Therefore, in the analysis given hereafter, $\Delta u_j = 5\%$ was considered.

V.B.2. Other Measuring Techniques

The prediction uncertainty based on the Li-pellet, Li-metal, and zonal measurements is shown in Figs. 12, 13, and 14, respectively. The number of cases, N, in these measurements is less than in the case of Li-glass measurements. The Gaussian distributions that approximate the NDFs are shown in Figs. 15 and 16. Table II gives the mean uncertainty, $\bar{u}$, the standard deviation, σ_u, the root mean square value, u_{rms}, and the most probable value, u_{mp}, as obtained from the constructed NDFs (not the Gaussians) for each measuring technique. These parameters are additionally given in Table II for the case of including only the calculational errors in the analysis. The pertaining parameters when all the cases in each measuring method are considered together in deriving the NDFs are also shown in the figures and table; that is, no distinction has been made among the measuring techniques.

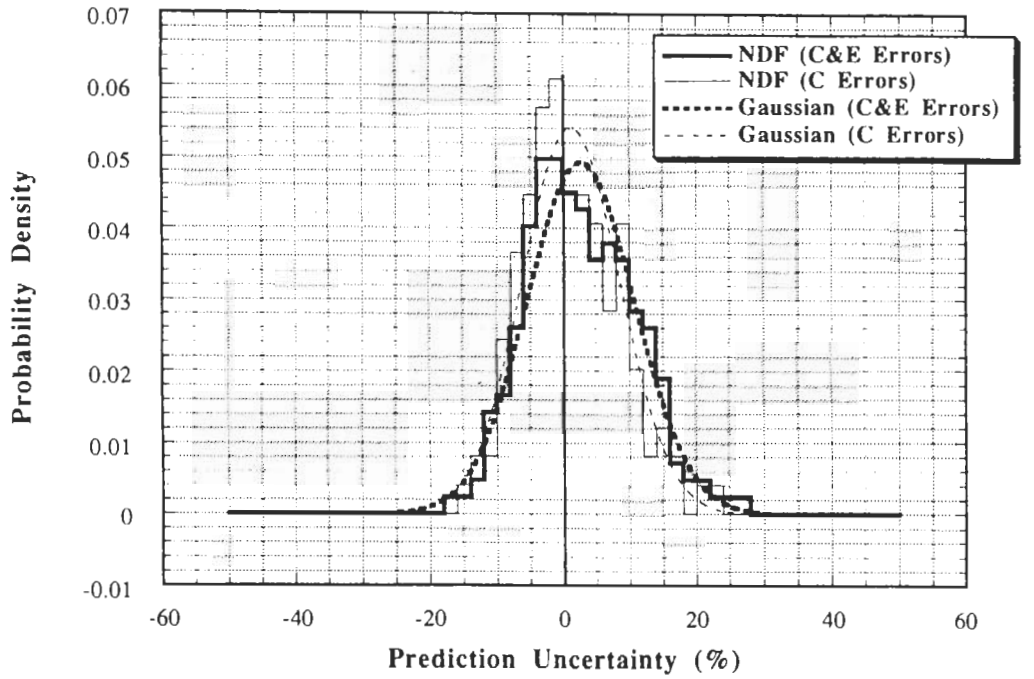

Fig. 7. Normalized density function of the prediction uncertainty of T_6 (U.S. codes and data—Li-glass measurements—all phases).

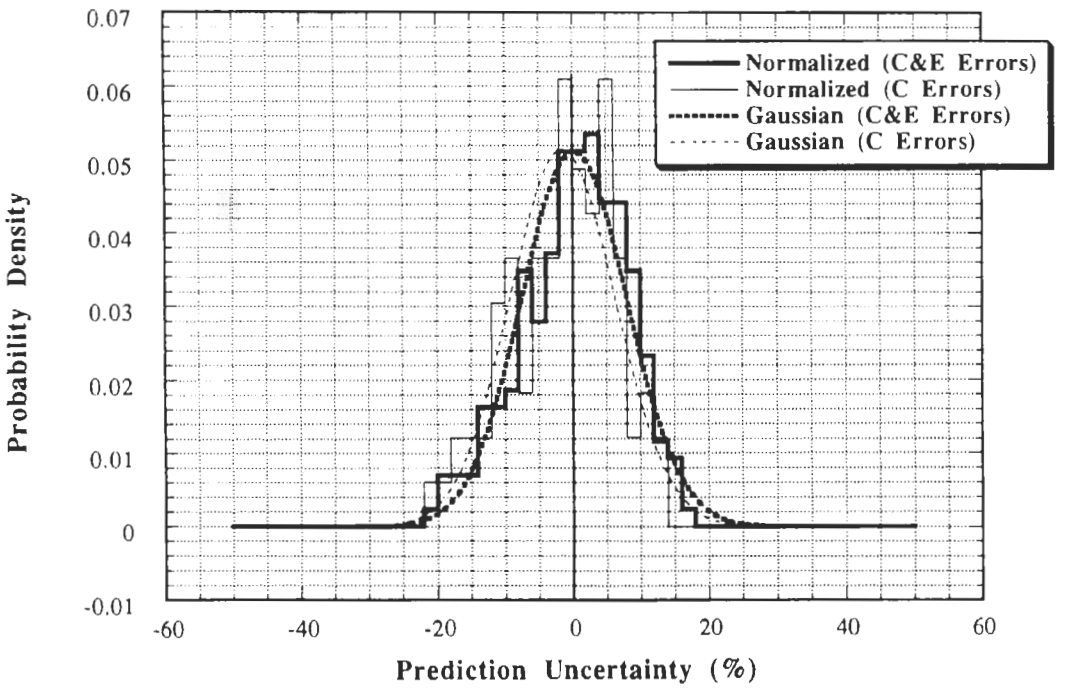

Fig. 8. Normalized density function of the prediction uncertainty of T_6 (JAERI's codes and data—Li-glass measurements—all phases).

According to Table II, the mean uncertainty, $\bar{u}$, in all cases is positive, even when the experimental errors are not accounted for (with one exception: Li-glass, JAERI, C errors only). This reflects that it is highly likely that the calculations performed to estimate T_6 production by blanket designers are larger than the actual measured values and this emphasizes the need to apply safety factors. The least uncertainty is obtained

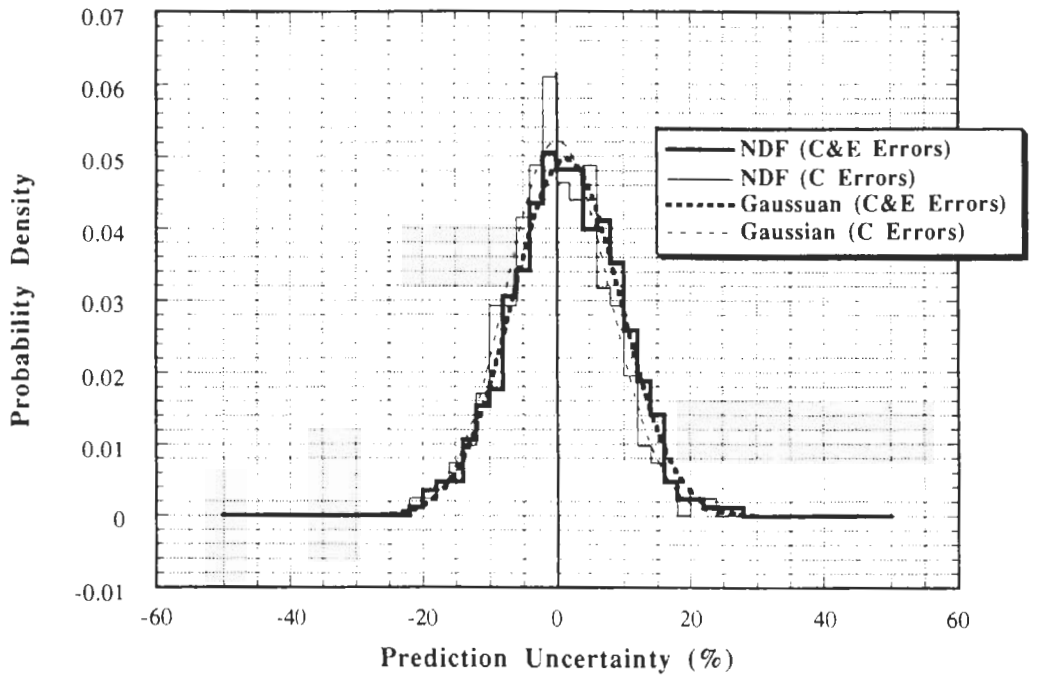

Fig. 9. Normalized density function of the prediction uncertainty of T_6 (U.S. and JAERI codes and data—Li-glass measurements—all phases).

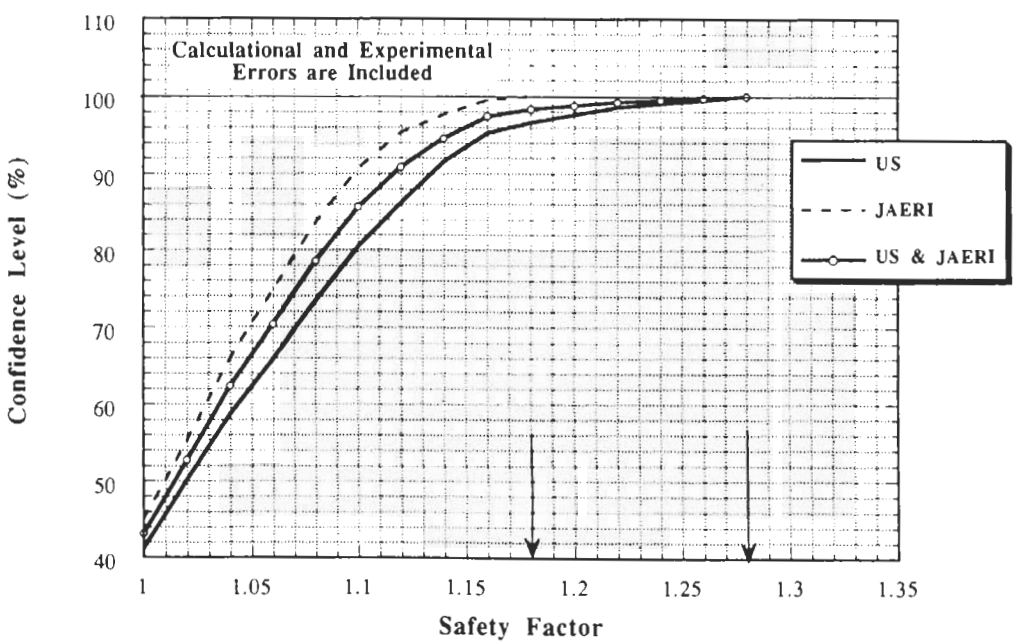

Fig. 10. Confidence level for calculations not to exceed measurements as a function of design safety factors for T_6 (all phases—Li-glass measurements—C&E errors are included).

with the Li-glass method and the largest uncertainty is obtained with the Li-pellet technique (Li-metal technique in JAERI's case). This is true also in the case of including only the C errors. The differences among these least and largest values are ~6%. If only the C errors are included, the differences among all techniques are ~8%, which could be qualitatively viewed as a conservative estimate to the differences found among various techniques in measuring T_6. However, the spread around the mean, σ_u, varies as 7.5 to 9.8%

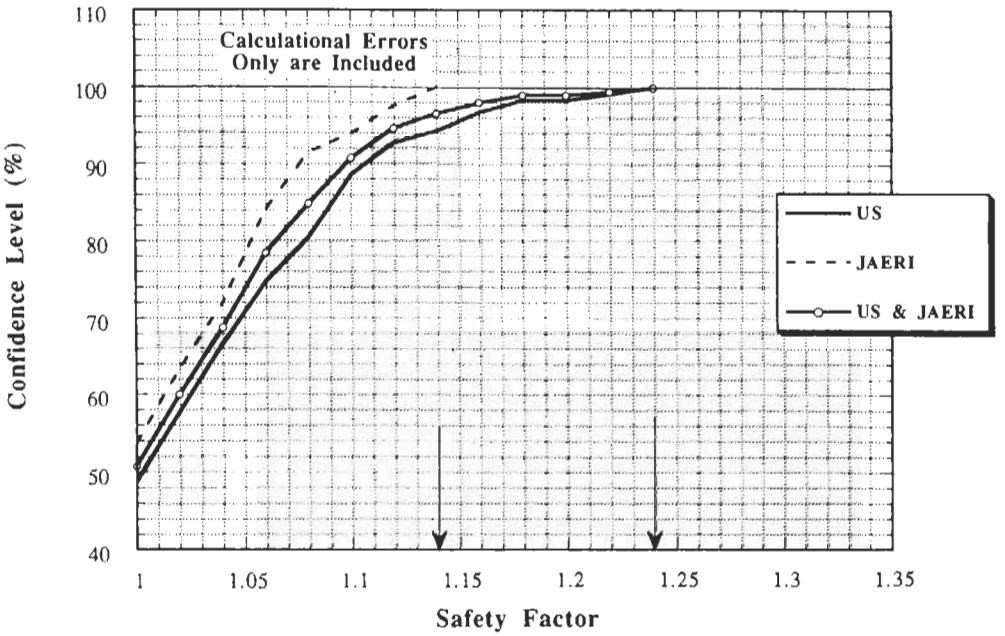

Fig. 11. Confidence level for calculations not to exceed measurements as a function of design safety factors for T_6 (all phases – Li-glass measurements – C errors only are included).

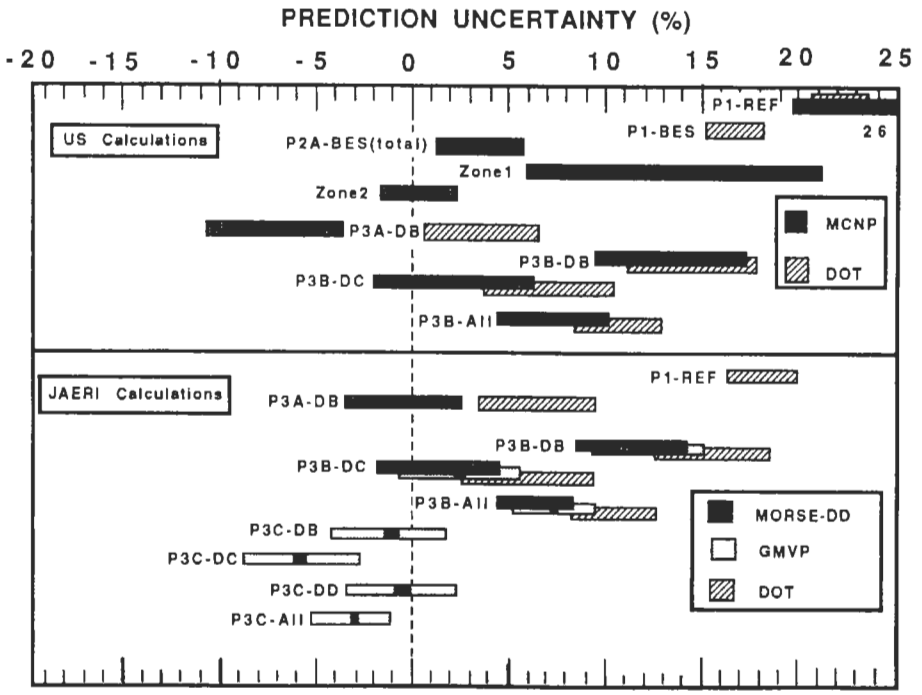

Fig. 12. The prediction uncertainty in the line-integrated TPR from Li-6 (T_6) (measurements: Li-pellet method).

(U.S.) and 3.7 to 11% (JAERI). This spread is ~7.9 to 9.7% (U.S.) and 3.9 to 12.4% (JAERI) in the case of including only the C errors, and thus, the differences among techniques in evaluating $\bar{u}$ fall within this spread in the prediction uncertainty.

When the cases considered in each measuring method are combined, the mean prediction uncertainty is ~5% (U.S.) and 2% (JAERI) with a standard deviation of ~9% (U.S.) and 8% (JAERI). These estimates are closer to (but larger by ~2% than) those obtained

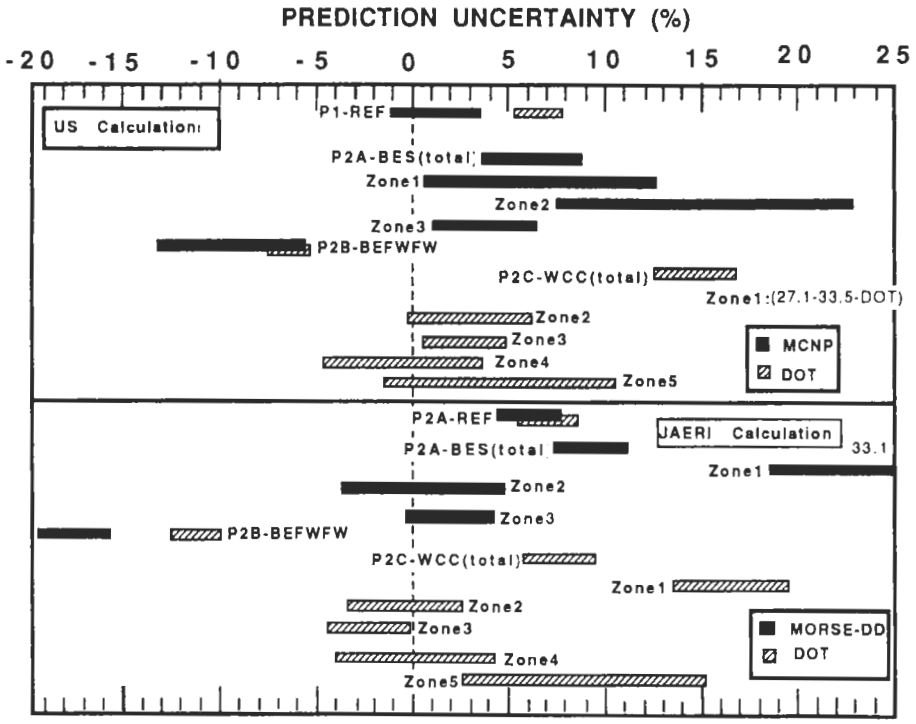

Fig. 13. The prediction uncertainty in the line-integrated TPR from Li-6 (T_6) (measurements: Li-metal method).

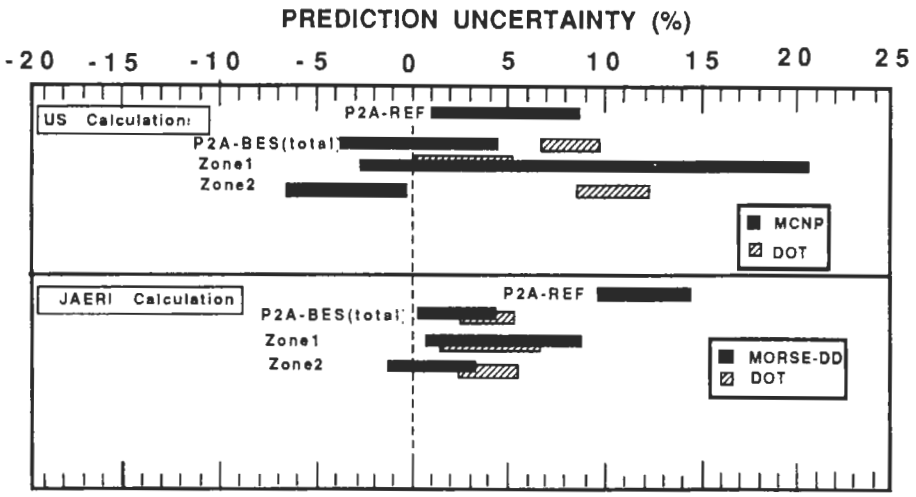

Fig. 14. The prediction uncertainty in the line-integrated TPR from Li-6 (T_6) (measurements: zonal method).

with the Li-glass method since the number of cases, N, considered with this technique is considerably larger than those accounted for in other methods. When all the results of the U.S. and JAERI (denoted U.S.&JAERI) are combined for all measuring techniques, the prediction uncertainty is ~3.5% with a standard deviation of ~8.8%. These values are somewhat between those obtained by the U.S. and JAERI when their cases are treated separately.

V.B.3. Design Safety Factors

Figures 17 and 18 give the design safety factors and the associated levels of confidence based, respectively, on the U.S. and the JAERI calculations. If no safety

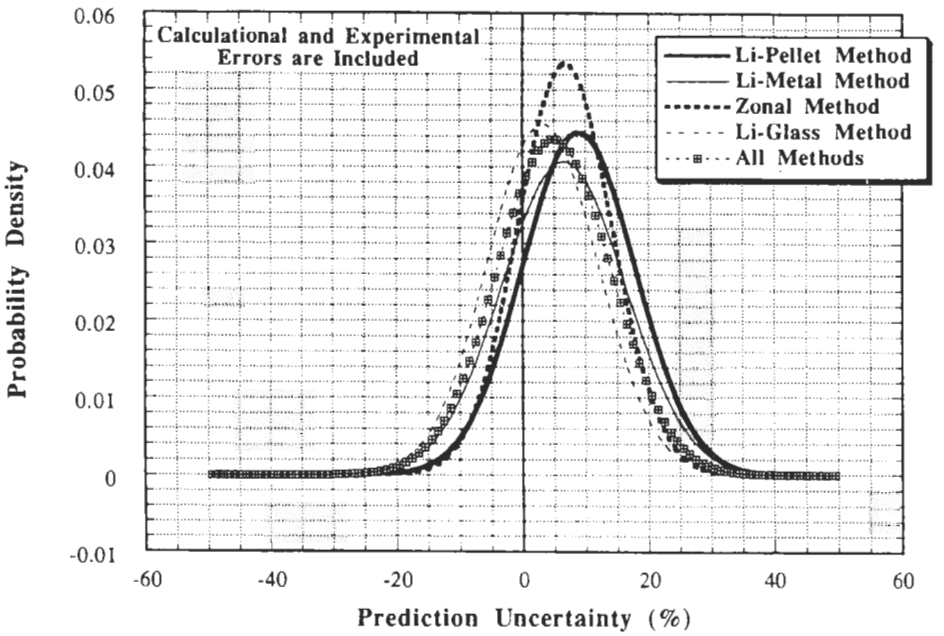

Fig. 15. Gaussian distributions that approximate the NDFs of the prediction uncertainties in T_6 measured by several methods (U.S. calculations).

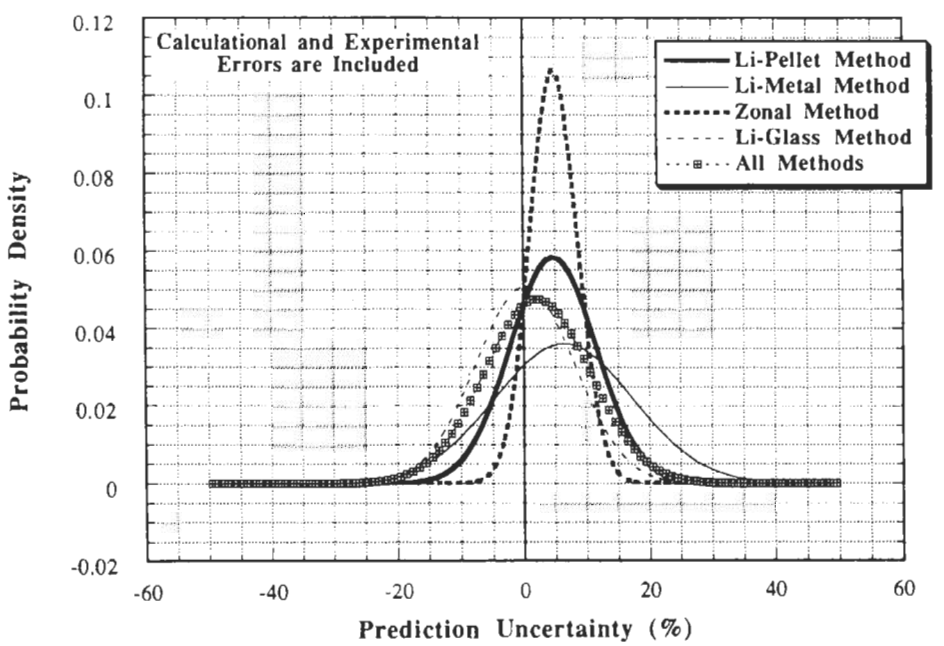

Fig. 16. Gaussian distributions that approximate the NDFs of the prediction uncertainties in T_6 measured by several methods (JAERI's calculations).

factors are used ($S_k = 1$), the confidence levels based on Li-glass, Li-metal, zonal, Li-pellet, and all measuring methods are respectively as follows:

~38, ~23, ~24, ~15, and ~30% (U.S.)
~45, ~27, ~8, ~28, and ~38% (JAERI)
~43, ~25, ~17, ~21, and ~34% (U.S.&JAERI).

The U.S.&JAERI results shown above are based on the constructed NDF (not shown) from the U.S. and the JAERI cases, combined together. All these confidence levels are lower than 50% indicating that the calculation of T_6 is overpredicted and the least overprediction (larger confidence level) is in the case of the Li-glass method. The largest overprediction is obtained by the

TABLE II

Statistical Parameters of the Prediction Uncertainty, u (%), of TPR from Li-6 (T_6) as Obtained from Various Experimental Methods

Method	Calculational and Experimental Error Included			Calculational Errors Only Included		
	U.S.	JAERI	U.S. & JAERI	U.S.	JAERI	U.S. & JAERI
Li-glass						
Number of cases considered	50	58	108	50	58	108
$\bar{u}$ (average)	3.17	0.22	1.63	2.05	−1.27	0.43
σ_u (standard deviation)	8.75	7.87	8.43	8.11	8.09	8.27
u_{rms} (root mean square)	9.31	7.87	8.58	8.36	8.19	8.28
u_{mp} (most probable)	0	2.5	2.5	−2.5	0	−2.5
Li-pellet						
Number of cases considered	15	16	31	15	16	31
$\bar{u}$ (average)	8.97	4.69	6.89	9.89	5.44	8.0
σ_u (standard deviation)	8.95	6.84	8.28	9.43	7.29	8.86
u_{rms} (root mean square)	12.67	8.28	10.77	13.66	9.10	11.94
u_{mp} (most probable)	7.5	5.0	7.5	5.0	−2.5	7.5
Li-metal						
Number of cases considered	14	14	28	14	14	28
$\bar{u}$ (average)	6.53	6.35	6.45	5.76	6.67	6.16
σ_u (standard deviation)	9.79	11.03	10.38	9.74	12.39	10.99
u_{rms} (root mean square)	11.77	12.73	12.22	11.31	14.07	12.60
u_{mp} (most probable)	2.5	2.5	2.5	2.5	7.5	5.0
Zonal						
Number of cases considered	7	7	14	7	7	14
$\bar{u}$ (average)	5.74	4.81	5.33	5.5	3.61	4.79
σ_u (standard deviation)	7.46	3.73	6.15	7.92	3.93	6.77
u_{rms} (root mean square)	9.41	6.08	8.14	9.64	5.34	8.29
u_{mp} (most probable)	7.5	2.5	5.0	2.5	2.5	2.5
All methods						
Number of cases considered	*86*	*95*	*181*	86	95	181
$\bar{u}$ (average)	*4.95*	*2.09*	*3.52*	4.35	1.3	2.95
σ_u (standard deviation)	*9.14*	*8.39*	*8.89*	9.09	9.21	9.27
u_{rms} (root mean square)	*10.39*	*8.65*	*9.56*	10.10	9.31	9.73
u_{mp} (most probable)	*2.5*	*2.5*	*2.5*	2.5	2.5	2.5

Li-pellet method (U.S.) and zonal method (JAERI). When all methods are accounted for, the confidence levels are closer to those obtained in the Li-glass case. The confidence levels in JAERI's case are larger than the ones based on the U.S. calculations. When results from the U.S. and JAERI are combined, the values of these levels are in between those of JAERI and the U.S. The most conservative safety factors based on Li-glass, Li-metal, zonal, Li-pellet, and all measuring methods are respectively:

1.30, 1.35, 1.26, 1.30, and 1.35 (U.S.)
1.20, 1.35, 1.16, 1.20, and 1.35 (JAERI)
1.30, 1.35, 1.26, 1.30, and 1.35 (U.S.&JAERI).

The Li-metal method gives the largest safety factors, and the least safety factors are obtained when measurements are performed with the zonal method. It should be emphasized that the number of cases considered using the zonal method is the least relative to the other measuring techniques and to verify that indeed this method gives the lowest safety factor at the 100% confidence level will require more measurements (cases) to be performed and added to those shown in Fig. 14.

V.B.4. Effect of Calculational Methods Applied

Distinction was made between the DO and MC calculational methods in evaluating the required safety factors in the case when results based on all measuring techniques are considered. Figures 19 and 20 show the NDF and the approximating Gaussian curves of the prediction uncertainty obtained from the DO and MC

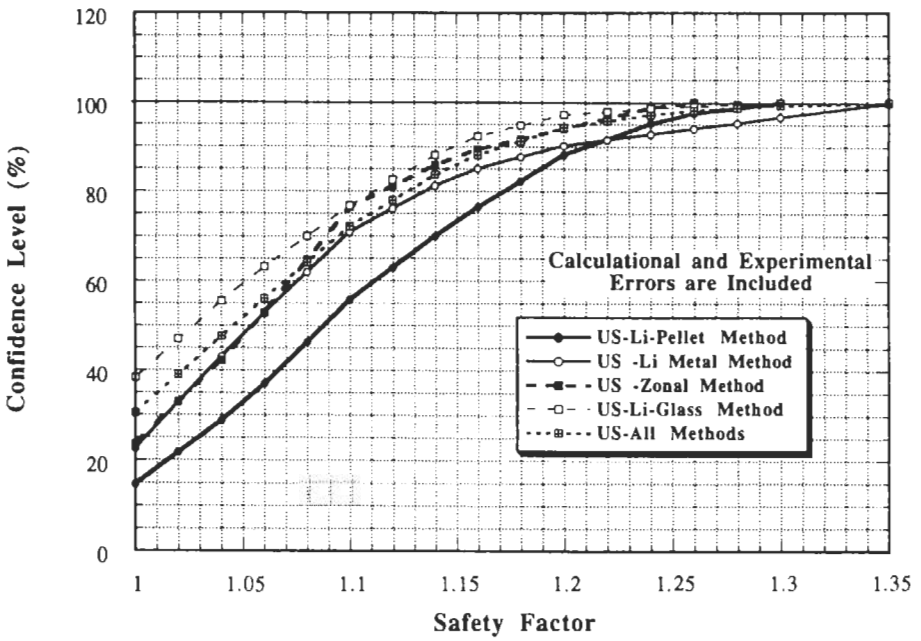

Fig. 17. Confidence level for the calculations not to exceed measurements as a function of the design safety factor for T_6 (U.S. calculations—all phases).

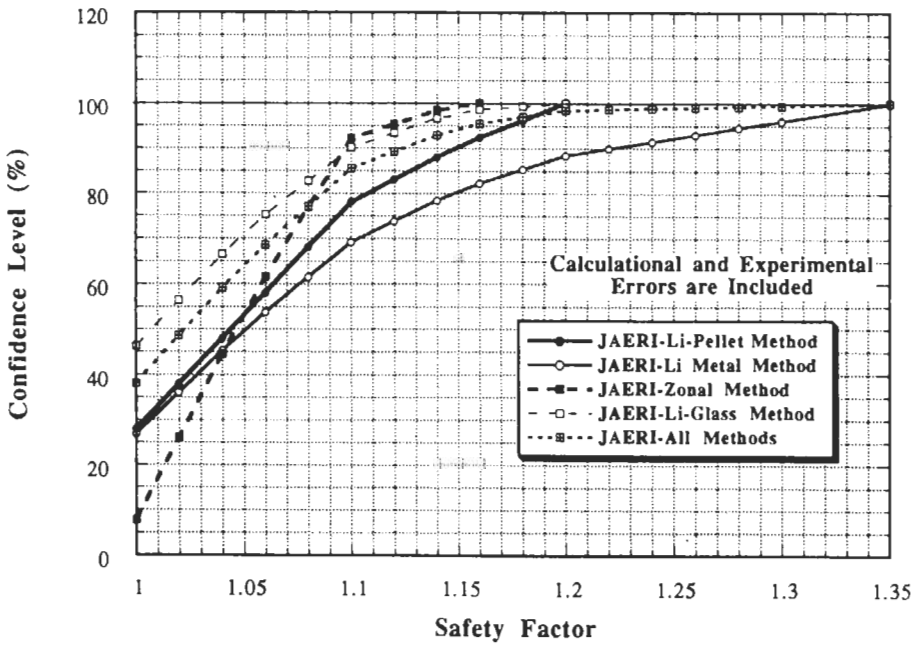

Fig. 18. Confidence level for the calculations not to exceed measurements as a function of the design safety factor for T_6 (JAERI calculations—all phases).

methods used by the U.S. and JAERI, respectively. The required safety factors as a function of the assigned confidence levels are shown in Figs. 21 and 22. Table III gives the pertaining statistical parameters ($\bar{u}$, σ_u, etc.) of the NDFs. The safety factors are summarized in Table IV for several confidence levels. Given also in Figs. 21 and 22 and in Table IV are these factors when the cases based on the two calculational methods are treated together.

From the U.S. calculations, the mean value, $\bar{u}$, based on the DO and MC methods is ~8 and ~2.6%, respectively, (as opposed to ~5% when both methods

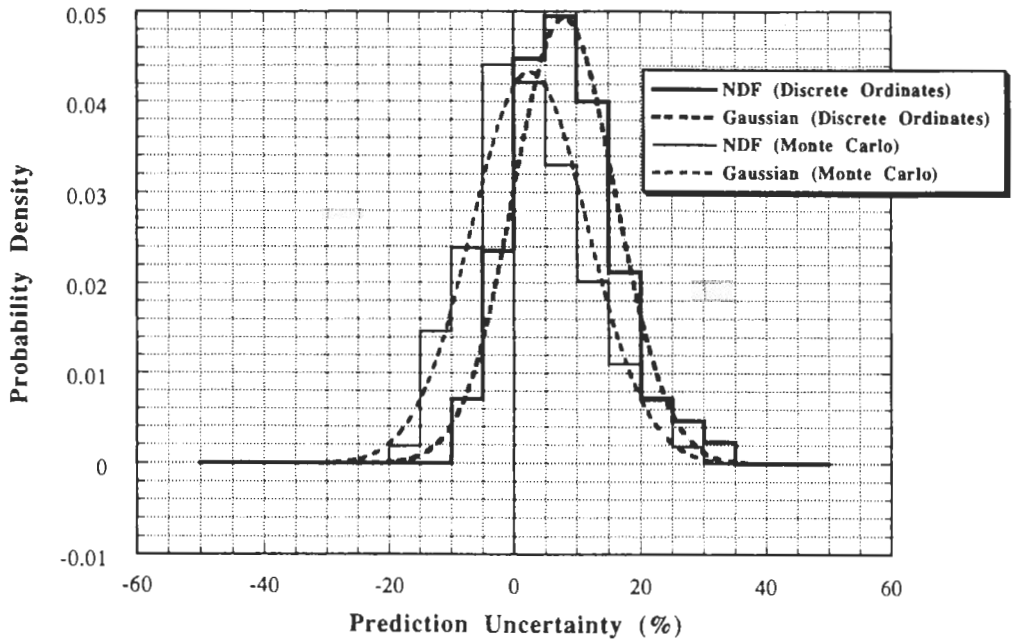

Fig. 19. Normalized density functions of the prediction uncertainties in T_6 constructed from the DO and MC calculations (U.S. calculations, all measuring methods, all phases).

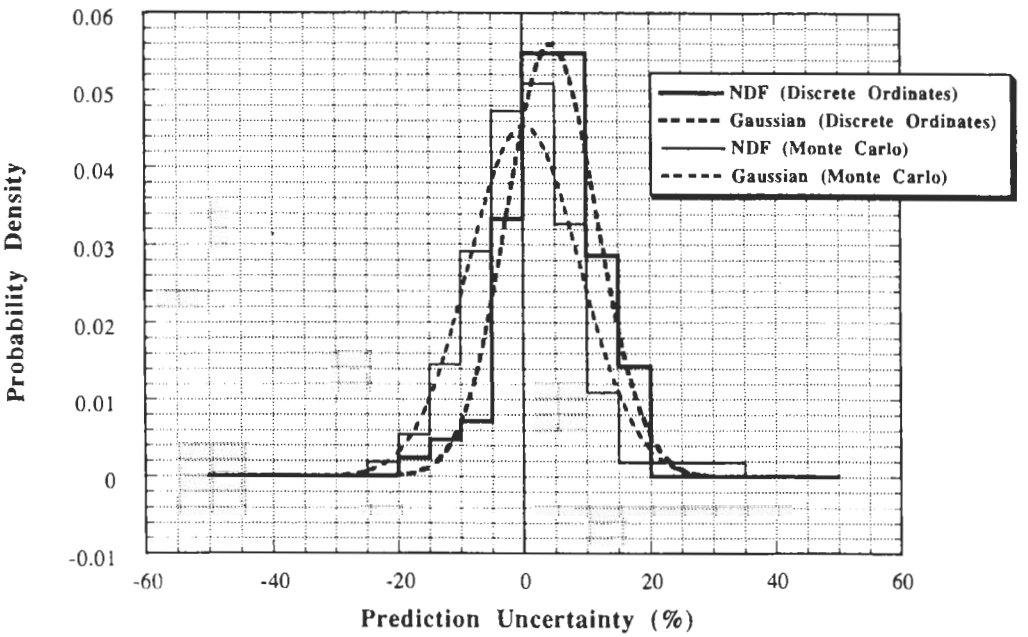

Fig. 20. Normalized density functions of the prediction uncertainties in T_6 constructed from the DO and MC calculations (JAERI calculations, all measuring methods, all phases).

are considered together) with a spread, σ_u, of ~8% and 9%, indicating that the DO method tends to give larger T_6 by ~5%. This is also true for the safety factors at various confidence levels where they are 3 to 6% larger in the DO case. In JAERI's calculation, $\bar{u}$ is 5% and 0.2% (as opposed to ~2% when both methods are considered together), with a spread of ~7% and 9% in the DO and MC cases, respectively. This again indicates that the DO method gives a larger mean T_6 by ~4.8% and larger safety factors by ~2 to 5%. In both

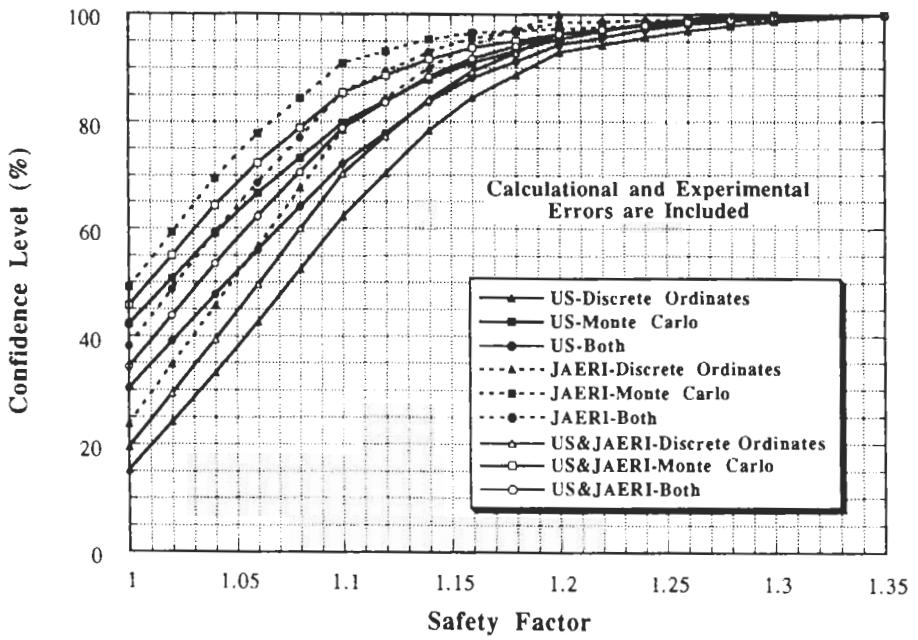

Fig. 21. Effect of the calculational method on the confidence levels and safety factors (T_6—all methods—all phases).

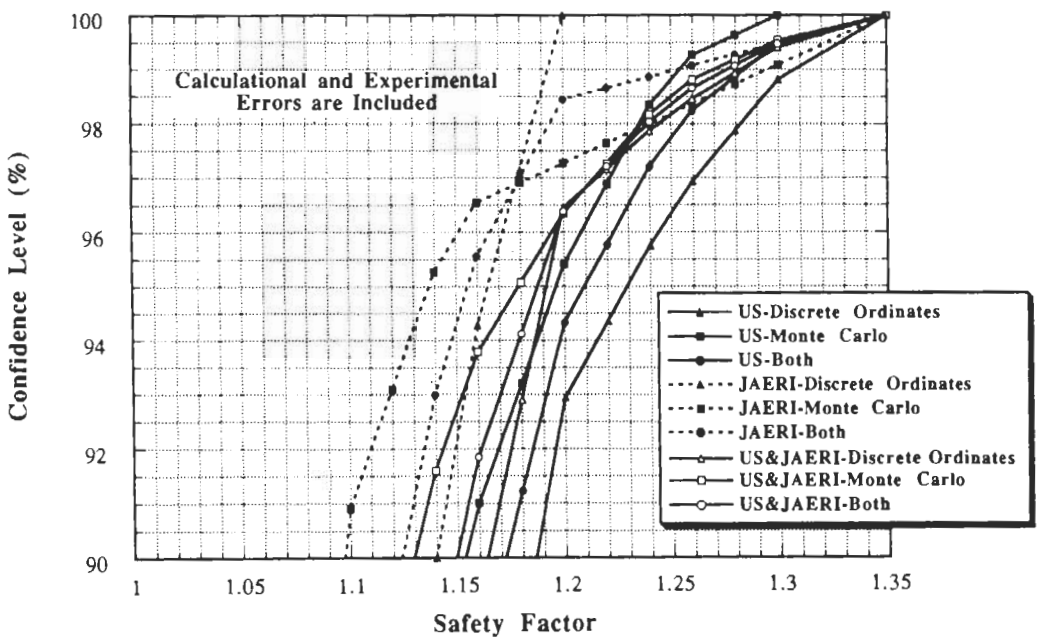

Fig. 22. Effect of the calculational method on the confidence levels and safety factors (T_6—all methods—all phases—confidence levels higher than 90%).

methods, the uncertainty, $\bar{u}$, based on the U.S. calculations is larger than JAERI's by 2 to 3% and the required safety factors are also larger by ~2 to 5%. When the U.S. and the JAERI cases are combined, the parameters, $\bar{u}$, σ_u, S_k, etc., have values that are in between those obtained by the U.S. and JAERI. One notices that the safety factors shown in Figs. 21 and 22 and given in Table IV increase by ~2% for every 10% increase in the confidence level, $(CL)_k$, up to $(CL)_k$ = ~90%. Beyond this value, the required safety factors change rapidly with $(CL)_k$.

V.C. The Prediction Uncertainties in the Line-Integrated TPR from Li-7 (T_7):

The prediction uncertainty in the line-integrated T_7, u_i, and the associated standard deviation, $\pm\sigma_i$, in

TABLE III

Statistical Parameters of the Prediction Uncertainty, u (%), of TPR as Obtained from Various Calculational Methods

Method	Discrete Ordinates Method			Monte Carlo Method		
	U.S.	JAERI	U.S. & JAERI	U.S.	JAERI	U.S. & JAERI
T-6 (all methods)						
Number of cases considered	43	42	85	43	53	96
$\bar{u}$ (average)	8.03	4.58	6.32	2.55	0.18	1.36
σ_u (standard deviation)	8.08	7.12	7.81	9.20	8.78	9.07
u_{rms} (root mean square)	11.39	8.47	10.05	9.55	8.78	9.17
u_{mp} (most probable)	7.5	5.0	7.5	−2.5	2.5	2.5
Design safety factor: (100% confidence)[a]	1.35	1.20	1.35	1.30	1.35	1.35
T-7 (all methods)						
Number of cases considered	40	39	79	39	50	89
$\bar{u}$ (average)	8.55	−0.89	3.96	2.03	0.02	0.94
σ_u (standard deviation)	9.65	7.95	10.04	10.63	10.46	10.59
u_{rms} (root mean square)	12.89	8.00	10.79	10.82	10.46	10.63
u_{mp} (most probable)	7.5	−7.5	2.5	5.0	−10.0	−7.5
Design safety factor: (100% confidence)	1.30	1.26	1.30	1.35	1.30	1.35
T-n (all methods)						
Number of cases considered	30	30	60	30	50	80
$\bar{u}$ (average)	6.50	3.06	4.87	2.34	−0.05	0.87
σ_u (standard deviation)	6.82	7.11	7.17	6.79	6.81	6.90
u_{rms} (root mean square)	9.42	7.74	8.67	7.18	6.82	6.96
u_{mp} (most probable)	5.0	2.5	2.5	2.5	−2.5	−2.5
Design safety factor: (100% confidence)	1.26	1.20	1.26	1.20	1.16	1.20

[a]Statistically, no such 100% confidence can be achieved (see text). These factors can be viewed as the largest values of C/E as evidenced from the analysis of all the experiments, considering both the experimental and calculational errors.

each experiment are shown in Figs. 23 and 24 using the NE213 method. The $\pm\sigma_i$'s are generally larger than those of T_6 and the uncertainty tends to have negative values as we proceed from Phase I to Phase III. The parameters u_i's and $\pm\sigma_i$'s are shown in Figs. 25, 26, and 27, respectively, in the cases of using the Li-pellet, Li-metal, and zonal techniques to measure T_7. The last two techniques were used in Phase II, and as shown, the prediction uncertainties are mostly negative, indicating that the measured values are larger than those obtained with the NE213 and Li-pellet methods. The experimental errors associated with the Li-pellet method are large in Phase III ($\geq$10%). The calculational errors of the Monte Carlo calculations performed by the GMVP code (JAERI) are smaller than those encountered in the MORSE-DD and MCNP calculations.

The Gaussian distributions that approximate the NDFs constructed from the cases given in Figs. 23 through 27 are shown in Figs. 28 and 29. Table V gives the relevant statistical parameters, and as in Table II, these parameters are also given for the case of considering only the calculational errors.

The mean uncertainty, $\bar{u}$, as predicted by the U.S. and JAERI, is negative in the case of zonal and Li-metal techniques as mentioned earlier. The uncertainty $\bar{u}$ is negative with the NE213 method in JAERI's calculation ($\bar{u} = -2\%$), while it is positive ($\bar{u} = 7.6\%$) in the U.S. calculations. In the U.S. case, the least uncertainty is obtained with the zonal method ($\bar{u} = -5.7\%$) and the largest is obtained with the Li-pellet method ($\bar{u} = 7.6\%$). This is also true in JAERI's case where the corresponding uncertainties are $\bar{u} = -11.6\%$ and $\bar{u} = 9.9\%$. Thus, the largest divergence due to differences among various measuring techniques is ~14% (U.S.) and ~22% (JAERI). When the C errors only are considered, this divergence is ~13% (U.S.) and ~21% (JAERI). The largest divergence in the case of combining the U.S. and the JAERI results is between the uncertainty predicted with the zonal method ($\bar{u} = -7.8\%$) and with the Li-pellet method ($\bar{u} = 9\%$), and it amounts to an overall difference of ~17%. In this later case, the spread around the mean uncertainty is $\pm$~6% with the zonal method and $\pm$~8% with the Li-pellet method, and thus there is little overlapping to cover the divergence of ~17%.

The largest standard deviation, σ_u, is ~11% (U.S., NE213) and ~9% (JAERI, Li-pellet), and the smallest is ~6.3% (U.S.) and ~3% (JAERI) with the zonal method. The largest and smallest σ_u are ~10 and 6% when the U.S. and the JAERI cases are combined, and similar to the mean uncertainties, these standard deviations fall between those of JAERI and the U.S., as

TABLE IV

Design Safety Factors for TPR as a Function of the Required Confidence Level

Level of Confidence	Tritium Production from Lithium-6 (T_6)			Tritium Production from Lithium-7 (T_7)			Tritium Production from Natural Lithium (T_n)		
	U.S.	JAERI	U.S. + JAERI	U.S.	JAERI	U.S. + JAERI	U.S.	JAERI	U.S. + JAERI
10%	1.00[a]	1.00	1.00	1.00	1.00	1.00	1.00	1.00	1.00
	1.00[b]	1.00	1.00	1.00	1.00	1.00	1.00	1.00	1.00
	1.00[c]	1.00	1.00	1.00	1.00	1.00	1.00	1.00	1.00
20%	1.00	1.00	1.00	1.00	1.00	1.00	1.00	1.00	1.00
	1.01	1.00	1.00	1.002	1.00	1.00	1.005	1.00	1.00
	1.00	1.00	1.00	1.00	1.00	1.00	1.00	1.00	1.00
30%	1.00	1.00	1.00	1.00	1.00	1.00	1.005	1.00	1.00
	1.03	1.00	1.02	1.03	1.00	1.00	1.03	1.00	1.00
	1.00	1.00	1.00	1.00	1.00	1.00	1.00	1.00	1.00
40%	1.02	1.01	1.01	1.02	1.00	1.00	1.02	1.00	1.01
	1.06	1.03	1.04	1.06	1.00	1.01	1.05	1.02	1.03
	1.00	1.00	1.00	1.00	1.00	1.00	1.01	1.00	1.00
50%	1.05	1.02	1.03	1.05	1.00	1.02	1.04	1.01	1.03
	1.08	1.05	1.06	1.08	1.00	1.03	1.07	1.03	1.04
	1.02	1.00	1.01	1.02	1.00	1.00	1.03	1.00	1.01
60%	1.08	1.04	1.06	1.08	1.02	1.05	1.06	1.03	1.05
	1.11	1.07	1.08	1.11	1.01	1.06	1.08	1.05	1.07
	1.05	1.02	1.03	1.05	1.03	1.04	1.04	1.02	1.03
70%	1.10	1.07	1.08	1.11	1.05	1.08	1.08	1.05	1.07
	1.13	1.09	1.10	1.15	1.03	1.09	1.11	1.07	1.09
	1.07	1.04	1.06	1.08	1.07	1.07	1.06	1.04	1.05
80%	1.13	1.09	1.11	1.15	1.08	1.12	1.11	1.08	1.09
	1.15	1.11	1.13	1.18	1.06	1.13	1.13	1.09	1.12
	1.10	1.07	1.08	1.11	1.10	1.10	1.09	1.07	1.06
90%	1.16	1.14	1.15	1.20	1.13	1.17	1.14	1.11	1.13
	1.19	1.14	1.17	1.22	1.10	1.19	1.16	1.13	1.15
	1.15	1.10	1.13	1.16	1.15	1.15	1.12	1.10	1.10
95%	1.21	1.16	1.19	1.24	1.17	1.21	1.17	1.13	1.15
	1.24	1.17	1.19	1.24	1.14	1.22	1.18	1.15	1.17
	1.20	1.14	1.18	1.21	1.19	1.20	1.13	1.12	1.13
100%[d]	1.35	1.35	1.35	1.35	1.30	1.35	1.26	1.20	1.26
	1.35	1.20	1.35	1.30	1.28	1.30	1.26	1.20	1.26
	1.30	1.35	1.35	1.35	1.30	1.35	1.20	1.16	1.20

[a]Based on DO and MC calculations.
[b]Based on DO calculations.
[c]Based on MC calculations.
[d]See footnote of Table III.

expected (see Table V). When only the C errors are included, these variances are slightly smaller (9.7% and 5.8%). In all cases, the uncertainties $\bar{u}$ and σ_u are larger in the case where the C&E errors are included than the values found in the case when only the C errors are considered.

As can be seen from Table V, the mean prediction uncertainties in the U.S. calculations are larger than those calculated for JAERI (except with the Li-pellet method) by ~6 to 10% in all the various measuring methods. The standard deviations are also larger by ~3 to 4%. When cases of all the methods are considered together, the prediction uncertainty becomes closer to the one obtained by the NE213 method since more cases are included with this technique relative to the other measuring methods. The mean prediction uncertainty

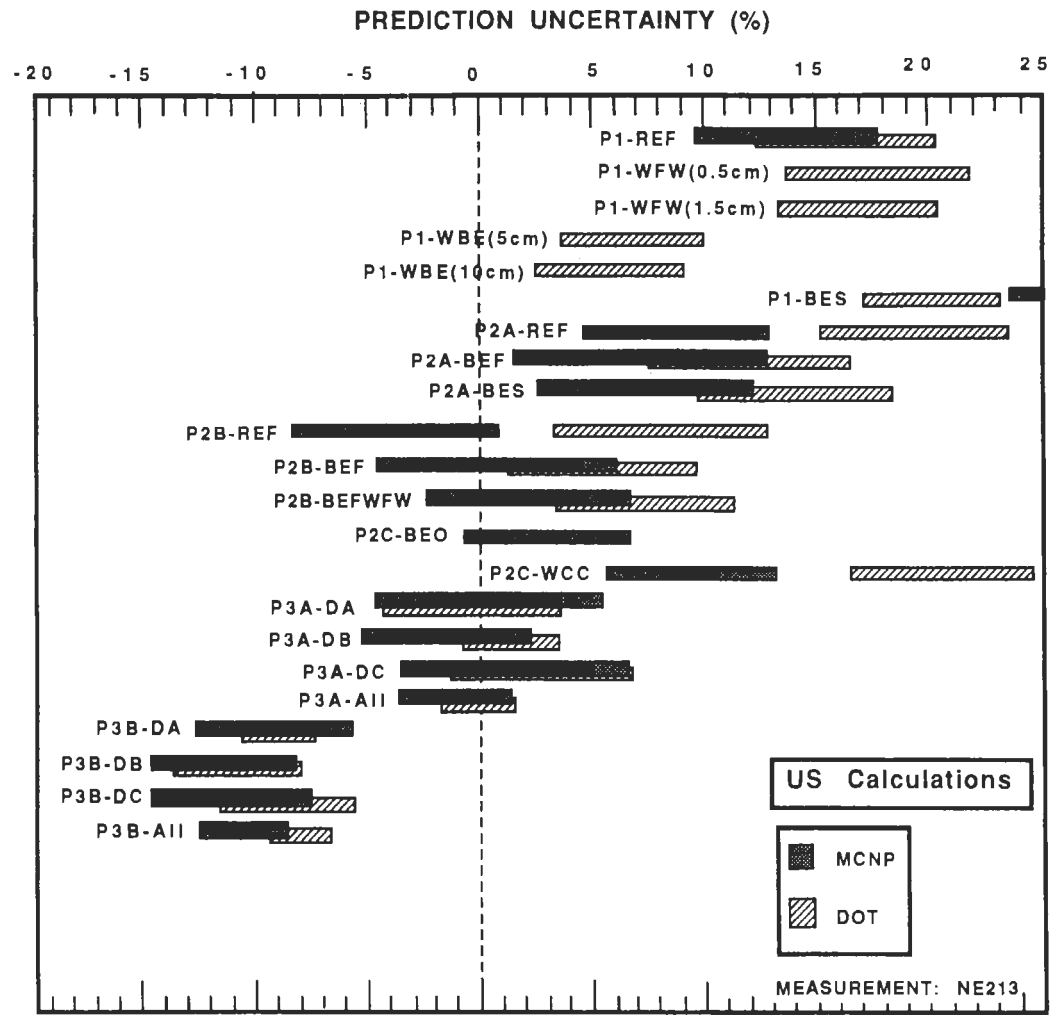

Fig. 23. The prediction uncertainty in TPR from Li-7 (T_7) (U.S. calculations, NE213 measurements).

is ~5% (U.S.) and −0.4% (JAERI) with a standard deviation of ~11% (U.S.) and 9.5% (JAERI); thus the U.S. values are larger than those of JAERI's by ~5% and ~2%, respectively.

V.C.1. Design Safety Factors

Figures 30 and 31 give the required design safety factors to be used in the TPR calculations of T_7 along with the associated levels of confidence based respectively on the U.S. calculations and JAERI's calculations. If no safety factors are used (S_k = 1), the confidence levels based on zonal, Li-metal, NE213, Li-pellet, and on all measuring methods are as follows:

~80, ~55, ~24, ~20, and ~32% (U.S.)
~100, ~95, ~60, ~15, and ~55% (JAERI)
~87, ~70, ~42, ~17, and ~44% (U.S.&JAERI).

We notice that the confidence levels are more than 50% in the case of the zonal and Li-metal methods. This means that the probability that the calculated T_7 is larger than the measured values is lower than 50%, implying that the mean value of the prediction uncertainty is negative in these two cases as was seen in Figs. 28 and 29. Also, the confidence level in JAERI's case with the zonal measurements is 100% at S_k = 1, indicating that the entire NDF falls in the negative space of the prediction uncertainty, u, as can be seen from Fig. 27. One should consider the results obtained with the zonal and Li-metal cautiously since few measurements were performed with these measuring techniques. As for the Li-pellet method, the confidence level is the lowest since most of the NDFs of both JAERI and the U.S. lie in the positive space of u and, therefore, the largest overprediction (least confidence level) is obtained by this measuring method. When all methods are accounted for, the confidence levels are closer to those obtained in the NE213 case. As it was shown for T_6, the confidence levels in JAERI's case are larger than the ones based on the U.S. calculations, e.g., for the same level of confidence, the required safety factors based on the U.S. calculations are larger than those based on

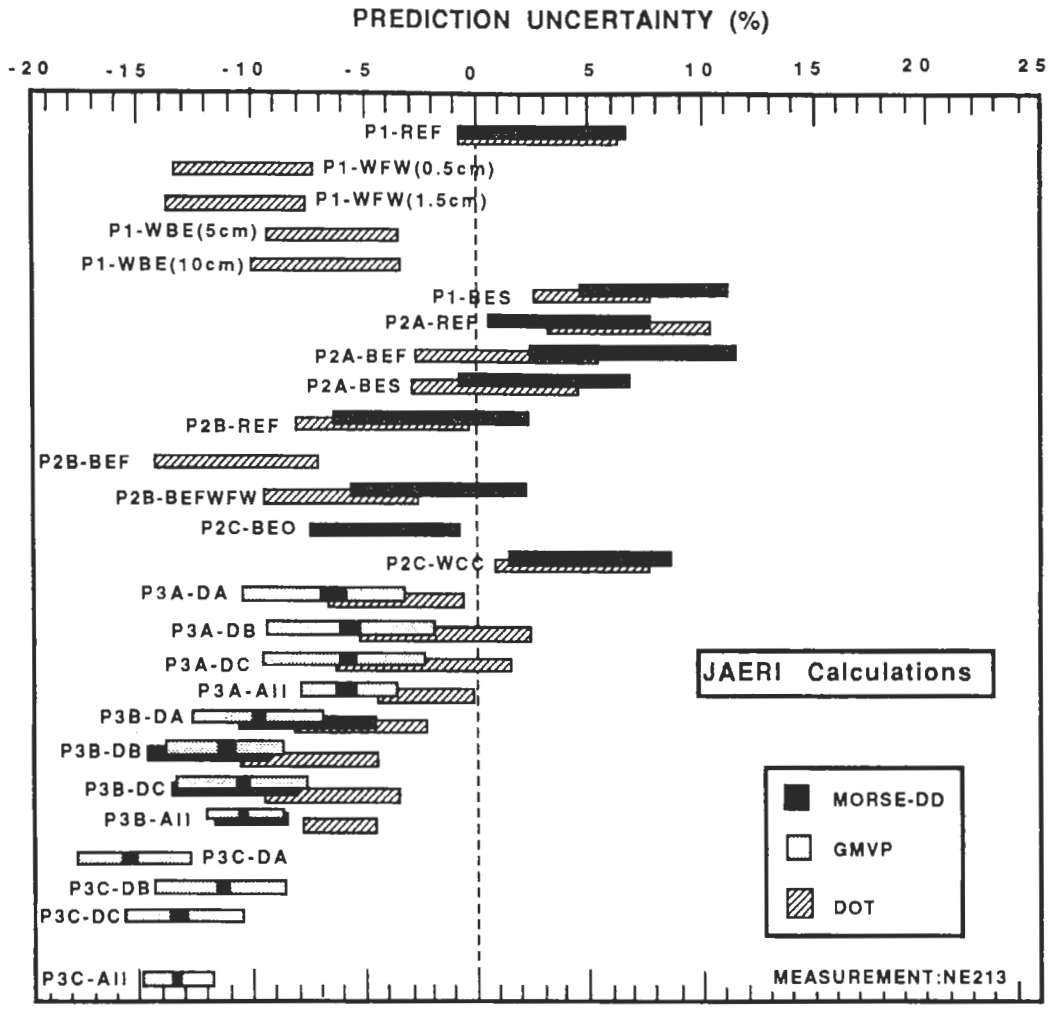

Fig. 24. The prediction uncertainty in TPR from Li-7 (T_7) (JAERI's calculations, NE213 measurements).

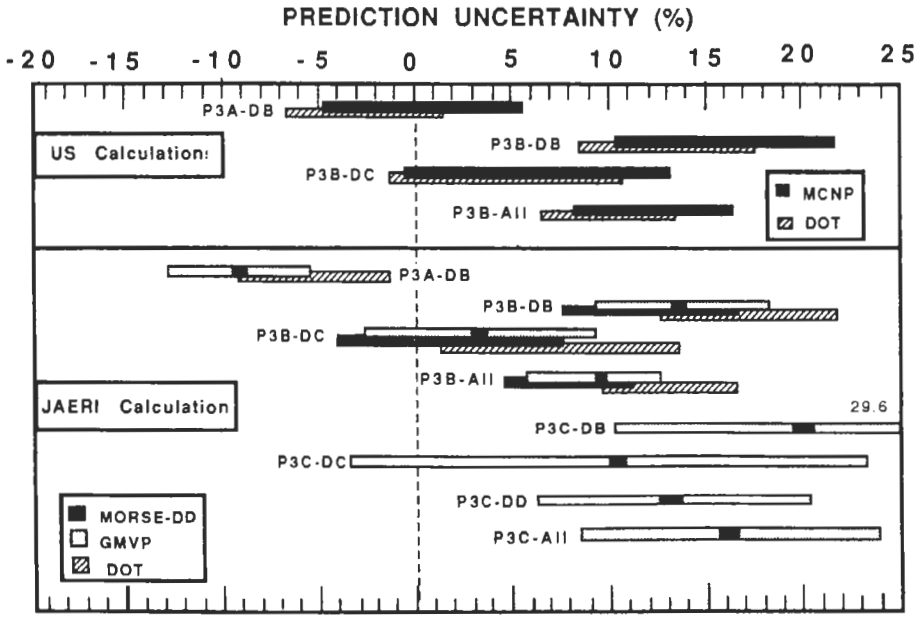

Fig. 25. The prediction uncertainty in TPR from Li-7 (T_7) (Li-pellet measurements).

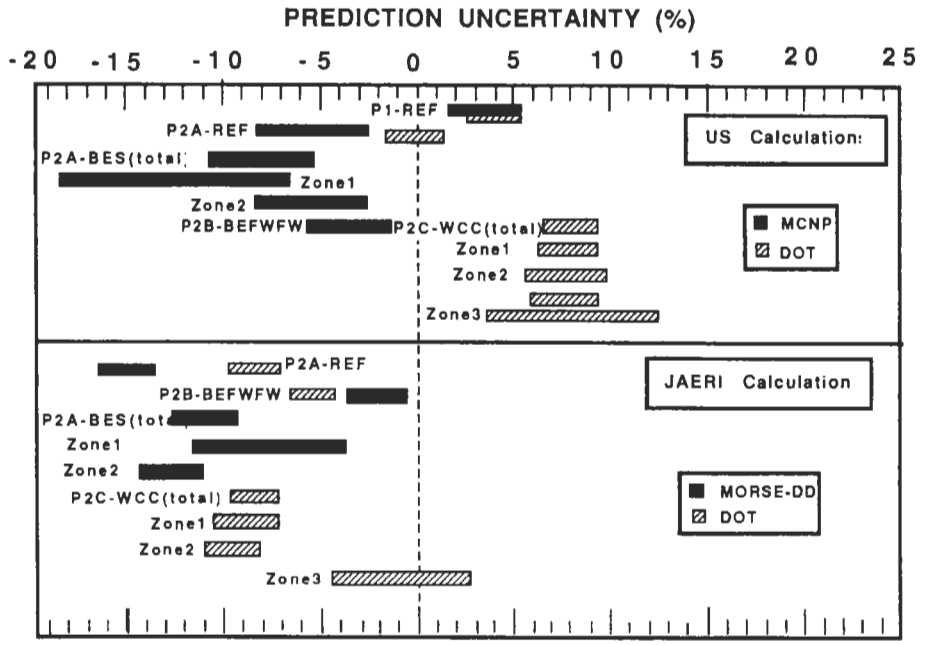

Fig. 26. The prediction uncertainty in TPR from Li-7 (T_7) (Li-metal measurements).

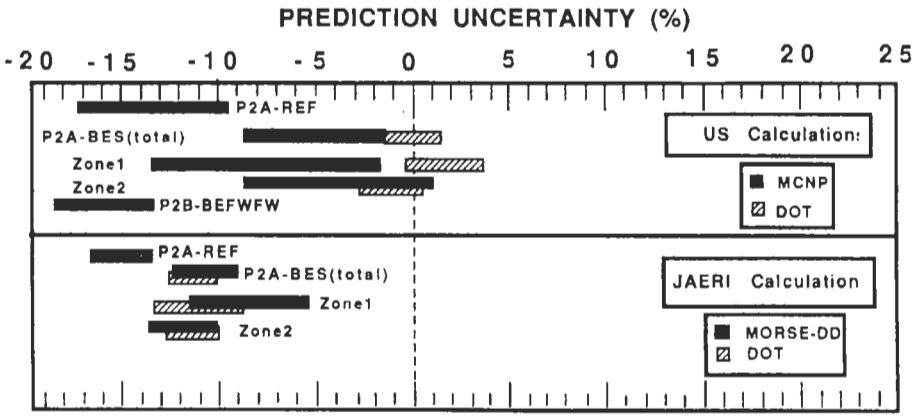

Fig. 27. The prediction uncertainty in TPR from Li-7 (T_7) (zonal measurements).

JAERI's calculations. When results from the U.S. and JAERI are combined, the values of these levels are in between those of the U.S. and JAERI. At the highest confidence level, the most conservative safety factors based on zonal, Li-metal, NE213, Li-pellet, and on all measuring methods are respectively as follows:

1.06, 1.16, 1.35, 1.26, and 1.35 (U.S.)
1.00, 1.06, 1.16, 1.30, and 1.30 (JAERI)
1.06, 1.16, 1.35, 1.30, and 1.35 (U.S.&JAERI).

Based on the U.S. calculations, the NE213 method requires larger safety factors as can generally be seen from Fig. 30 for confidence levels >50%. In JAERI's case, the highest safety factors required among the various techniques are those based on the Li-pellet measurements. This is consistent with the earlier discussion related to Table V. The reason for these large safety factors can be referred to from Fig. 25, where the prediction uncertainties, u_i's, and the standard deviations, σ_i's, are large in JAERI's calculation for T_7 in phase IIIC, leading to a large mean prediction uncertainty, $\bar{u}$, and large standard deviation, σ_u, in the constructed NDF. These Phase IIIC cases were not considered by the U.S. Additionally, one can see from Figs. 23 and 24 that the prediction uncertainties, u_i's, obtained with the NE213 method are negative based on JAERI's calculations in all Phase III experiments (including the cases of Phase IIIC, which were not considered by the U.S.). This led to smaller safety factors in JAERI's case based on the NE213 measurements. The least safety

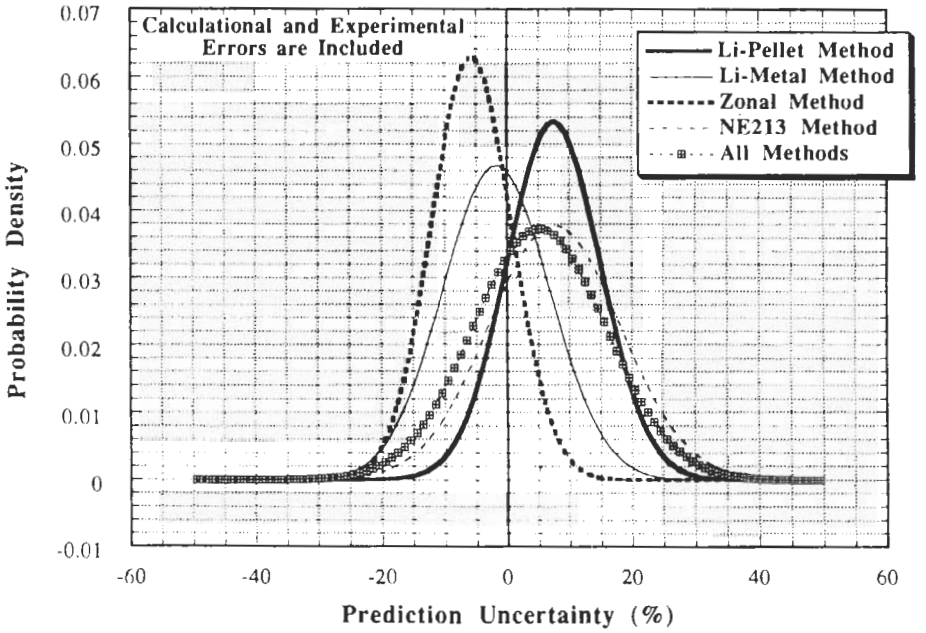

Fig. 28. Gaussian distributions that approximate the NDFs of the prediction uncertainties in T_7 measured by several methods (U.S. calculations).

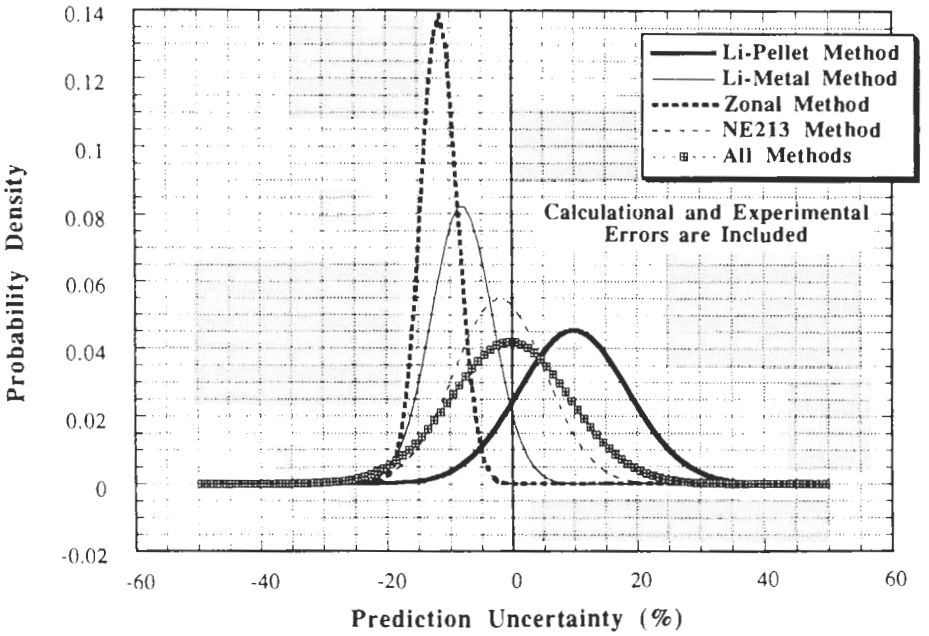

Fig. 29. Gaussian distributions that approximate the NDFs of the prediction uncertainties in T_7 measured by several methods (JAERI's calculations).

factors are obtained when measurements are performed with the zonal method. This does not imply that this measuring technique is the best relative to the other techniques since measurements were performed in a small number of cases. It is highly recommended to pursue this technique in several future experiments to further examine the observation noted here.

V.C.2. Effect of Calculational Methods Applied

Figures 32 and 33 give the NDF and the approximating Gaussian curves of the prediction uncertainty in T_7 based on the independent DO and MC calculations of the U.S. and JAERI, respectively. Derived safety factors from the NDFs as a function of the

TABLE V

Statistical Parameters of the Prediction Uncertainty, u (%), of TPR from Li-7 (T_7) as Obtained from Various Experimental Methods

Method	Calculational and Experimental Error Included			Calculational Errors Only Included		
	U.S.	JAERI	U.S. & JAERI	U.S.	JAERI	U.S. & JAERI
NE213						
Number of cases considered	49	56	105	49	56	105
$\bar{u}$ (average)	7.58	−1.99	2.69	5.0	−3.47	1.14
σ_u (standard deviation)	10.54	7.28	10.21	9.91	7.23	9.75
u_{rms} (root mean square)	12.98	7.55	10.56	11.09	8.02	9.81
u_{mp} (most probable)	7.50	−7.50	2.5	5.0	−10.0	2.5
Li-pellet						
Number of cases considered	8	15	23	8	15	23
$\bar{u}$ (average)	7.5	9.9	9.08	6.67	9.26	8.19
σ_u (standard deviation)	7.48	8.78	8.43	6.07	8.03	7.4
u_{rms} (root mean square)	10.59	13.23	12.39	9.01	12.26	11.03
u_{mp} (most probable)	10.0	10.0	10.0	7.5	12.5	12.5
Li-metal						
Number of cases considered	14	11	25	14	11	25
$\bar{u}$ (average)	−1.73	−8.03	−4.39	−3.69	−8.65	−5.59
σ_u (standard deviation)	8.51	4.84	7.84	8.15	4.0	7.28
u_{rms} (root mean square)	8.69	9.37	8.98	8.95	9.53	9.18
u_{mp} (most probable)	7.5	−7.5	−7.5	−7.5	−7.5	−7.5
Zonal						
Number of cases considered	8	7	15	8	7	15
$\bar{u}$ (average)	−5.66	−11.59	−7.83	−6.56	−12.0	−8.65
σ_u (standard deviation)	6.33	2.87	6.05	6.43	2.69	5.93
u_{rms} (root mean square)	8.49	11.94	9.89	9.19	12.3	10.49
u_{mp} (most probable)	−2.5	−12.5	−12.5	−5.0	−12.5	−12.5
All methods						
Number of cases considered	*79*	*89*	*168*	79	89	168
$\bar{u}$ (average)	*5.11*	*−0.36*	*2.28*	2.17	−2.84	−0.1
σ_u (standard deviation)	*10.69*	*9.5*	*10.46*	10.1	9.08	9.97
u_{rms} (root mean square)	*11.85*	*9.51*	*10.7*	10.33	9.52	9.97
u_{mp} (most probable)	*7.5*	*−7.5*	*5.0*	5.0	−7.5	−7.5

assigned confidence levels are shown in Figs. 34 and 35. Table III also gives the statistical parameters ($\bar{u}$, σ_u, etc.) obtained from the constructed NDFs and the required safety factors are summarized in Table IV for several confidence levels.

From the U.S. calculations, the mean value, $\bar{u}$, of T_7 based on the DO and MC methods is ~8.6% and ~2%, respectively (as opposed to ~5% when both methods are considered together, see Table V), with a spread, σ_u, of ~9.7% and 10.6%. These values are similar to the corresponding ones calculated for T_6 (with slightly larger standard deviations). It is also true in this case that the DO method tends to give larger prediction uncertainty by ~6%. This larger overestimation necessitates using larger safety factors by ~3 to 6% at various confidence levels as shown in Table IV. These features are the same for T_6. In particular, it is worth noting that the required safety factors are almost identical to those of T_6 up to confidence level of ~50% beyond which the safety factors tend to be larger for T_7.

In JAERI's case, $\bar{u}$ is −0.9 and 0.02% based on the DO and MC calculations (as opposed to about −0.4% when both methods are considered together) with a spread of ~8 and 10%, respectively. In contrast to the T_6, the MC calculations tend to give slight overprediction while underprediction occurs based on the DO method. This is reflected on the required safety factors where they are larger (by ~2 to 4%) when derived from the MC calculations. The reason for having this feature is due to the large prediction uncertainty and very large standard deviation ($\pm\sigma$ of 15%, see Fig. 25) found when the MC results of the Li-pellet measurements in Phase IIIC are included in the analysis. Notice also from Tables III and IV that the mean

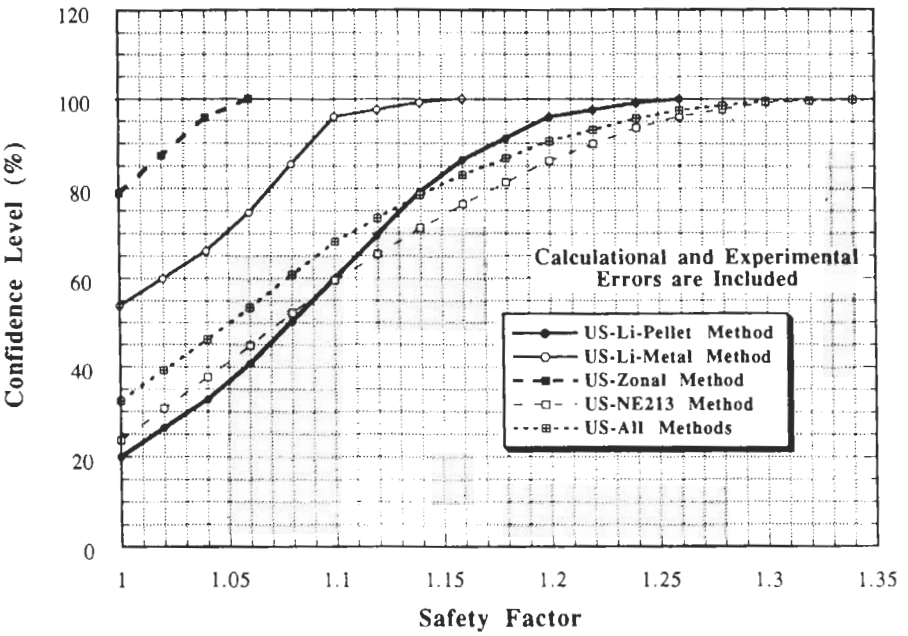

Fig. 30. Confidence level that calculations will not exceed measurements as a function of the design safety factor for T_7 (U.S. calculations – all phases).

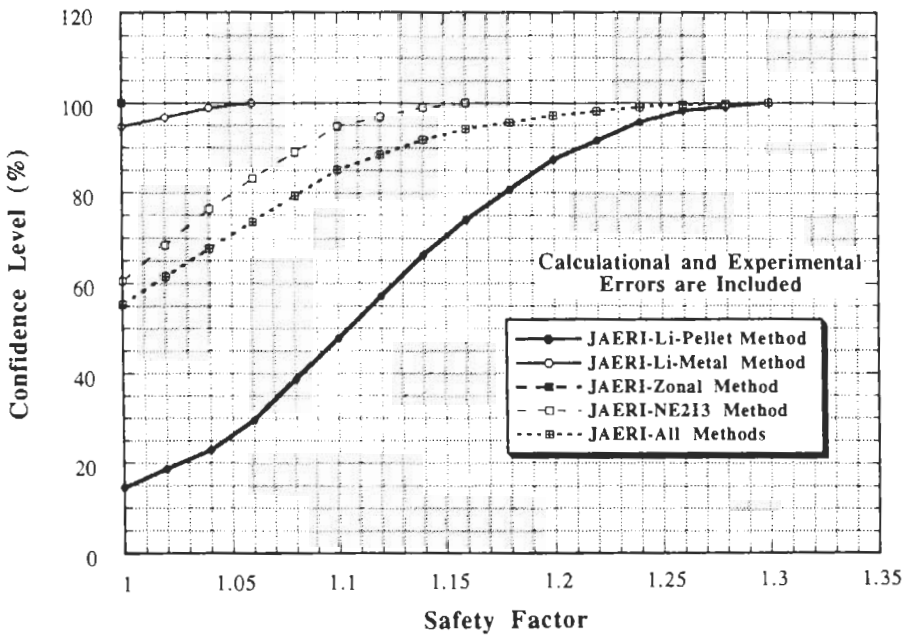

Fig. 31. Confidence level that calculations will not exceed measurements as a function of the design safety factor for T_7 (JAERI's calculations – all phases).

prediction uncertainty in the U.S. case is larger than that of JAERI by ~9% when the DO method is used and by ~2% based on the MC results. Consequently, the safety factors based on the DO method are larger than those of JAERI by ~6 to 11% and the factors based on the MC method are larger by ~1 to 2%. When the U.S. and the JAERI cases are combined, the parameters, $\bar{u}$, σ_u, S_k, etc., have values that are in between those obtained by the U.S. and JAERI. It can also be seen from Table IV that the safety factors increase by ~2 to 4% for every 10% increase in the confidence level, $(CL)_k$, up to $(CL)_k$ = ~90%. Beyond this value, the required safety factors change rapidly with $(CL)_k$.

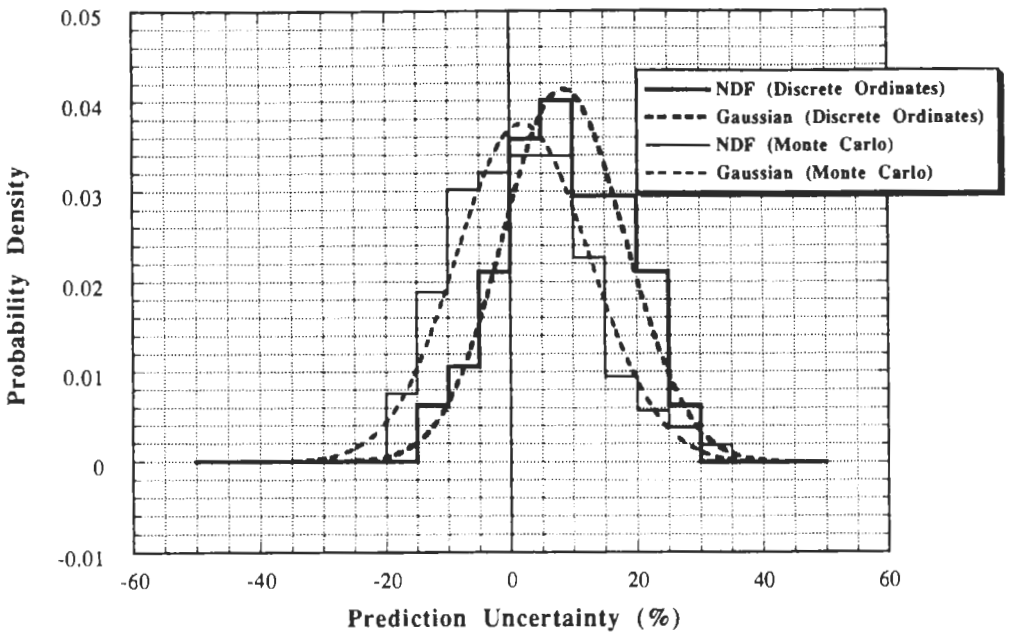

Fig. 32. Normalized density functions of the prediction uncertainties in T_7 constructed from the DO and MC calculations (U.S. calculations, all measuring methods, all phases).

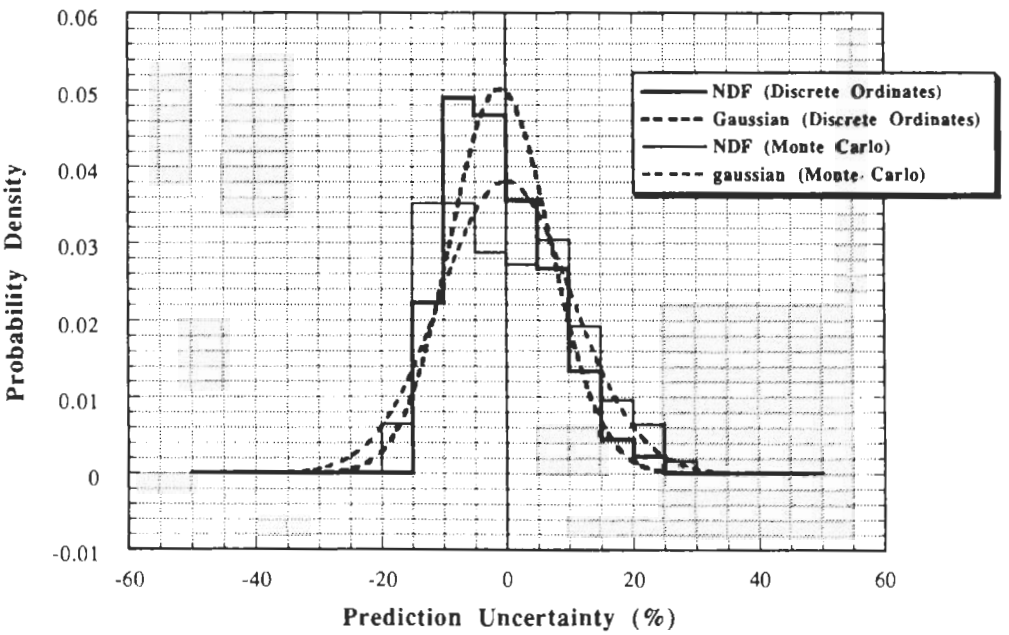

Fig. 33. Normalized density functions of the prediction uncertainties in T_7 constructed from the DO and MC calculations (JAERI calculations, all measuring methods, all phases).

V.D. The Prediction Uncertainties in Line-Integrated TPR from Natural Lithium (T_n)

The prediction uncertainty, u_i, and the standard deviation, σ_i, in the integrated TPR from natural lithium are shown in Fig. 36 with several measuring methods. The composed method refers to composing the local T_6 measured by the Li-glass method and the local T_7 measured by the NE213 method at a given spatial location to arrive at a measured value for T_n. Line integrations were then performed for the composed values of T_n. Figures 37 and 38 show the parameters, u_i

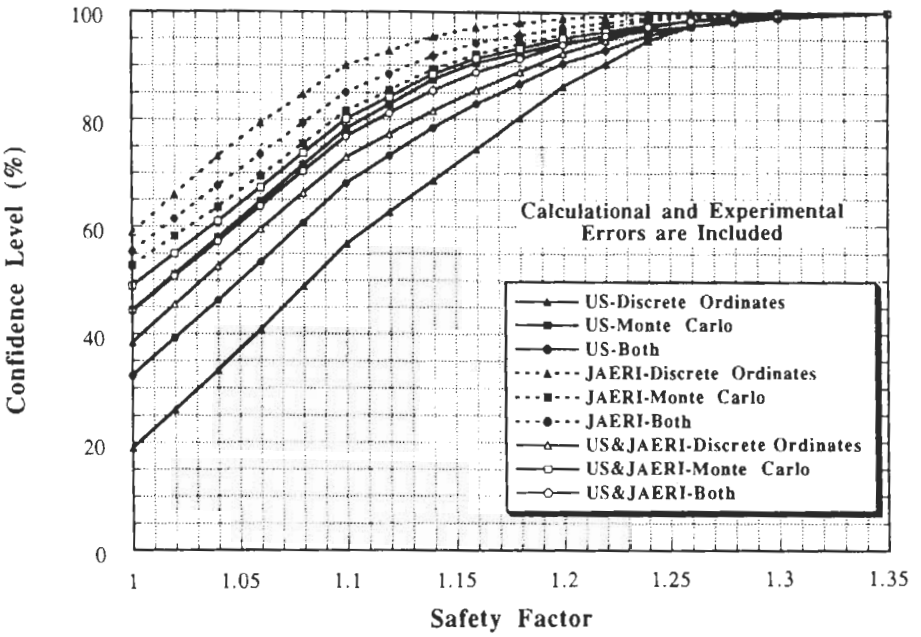

Fig. 34. Effect of the calculational method on the confidence levels and safety factors (T_7—all methods—all phases).

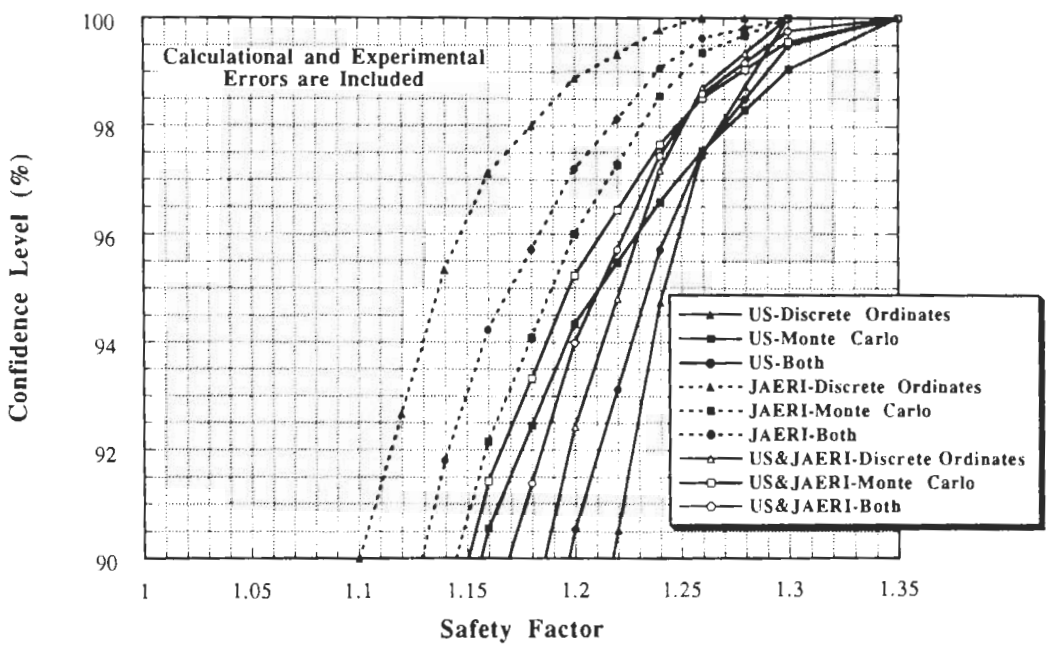

Fig. 35. Effect of the calculational method on the confidence levels and safety factors (T_7—all methods—all phases—confidence level above 90%).

and σ_i, but in the cases where the uncertainties and deviations are derived from those of T_6 measured by the Li-glass method and those of T_7 measured by the NE213 method according to Eqs. (24) through (27). This method of deriving the uncertainty in T_n is labeled (T6&T7) in these and other subsequent figures. Zonal measurements were performed in Phase II while Li-pellet measurements were carried out in Phase III. One notices that the uncertainties are positive in Phases IIIA and IIIB, while they have negative values in Phase IIIC when the Li-pellet method is used. (No cases were considered by the U.S. in Phase IIIC.) This observation could be due the existence of some systematic errors associated with the Li-pellet measurements in Phase IIIC.

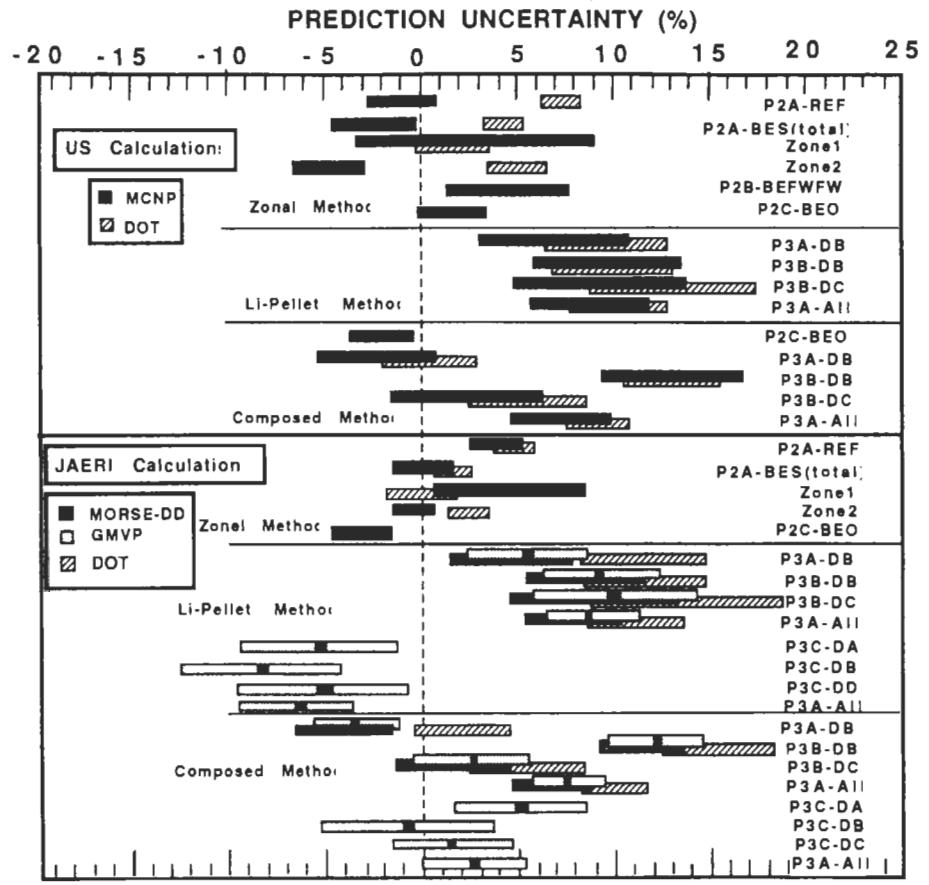

Fig. 36. The prediction uncertainty in TPR from natural lithium (T_n) (several measuring methods).

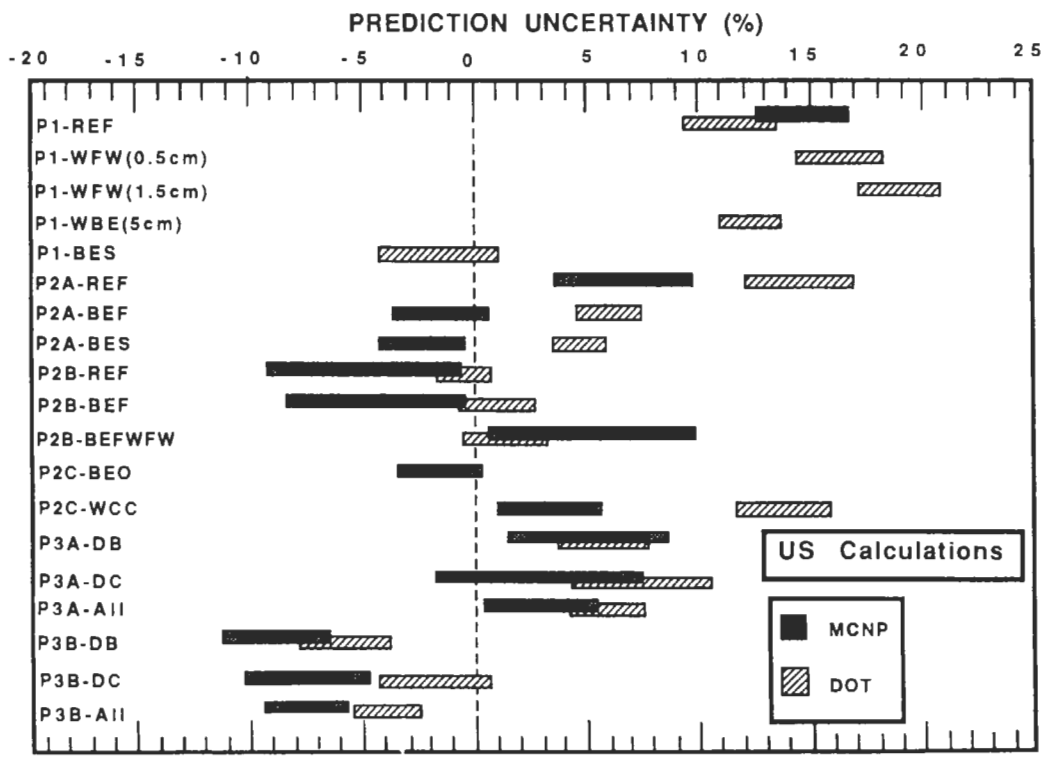

Fig. 37. The prediction uncertainty in TPR from natural lithium (T_n) (U.S. calculations—Li-glass and NE213 measurements).

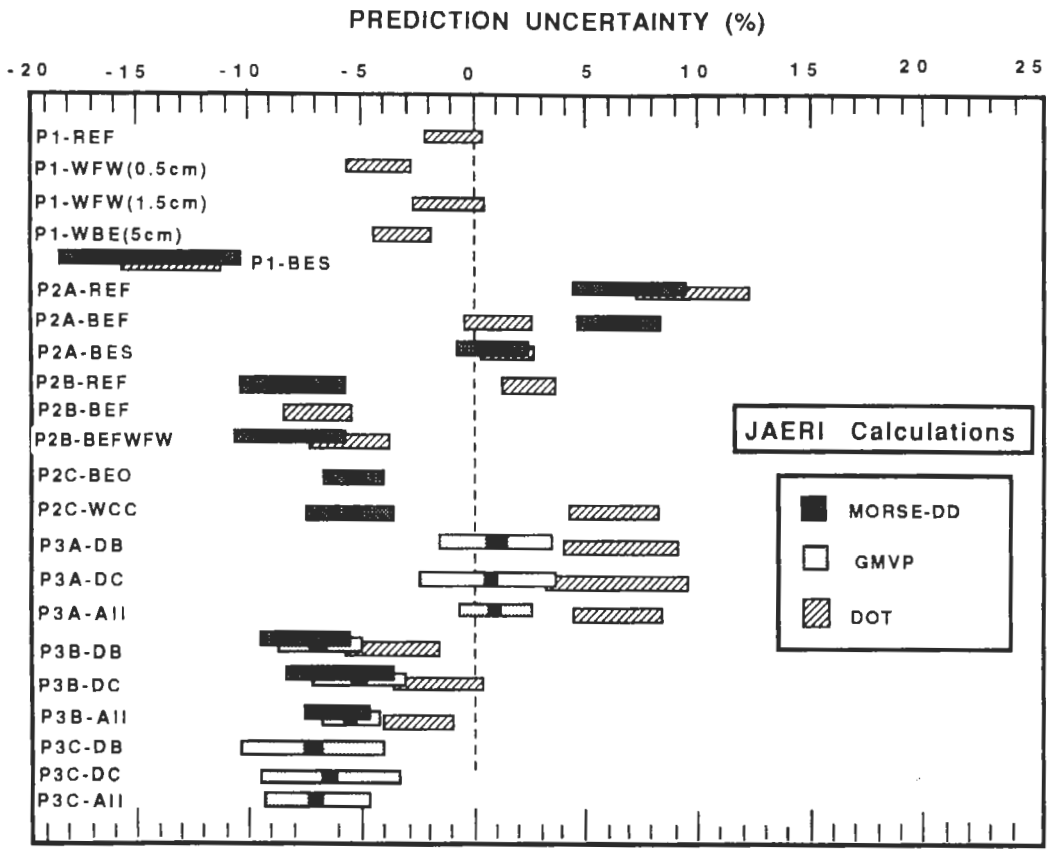

Fig. 38. The prediction uncertainty in TPR from natural lithium (T_n) (JAERI's calculations – Li-glass and NE213 measurements).

This also led to a wider NDF in JAERI's case (see Fig. 29). The constructed NDF based on this technique is narrower in the U.S. case with positive uncertainties since no counterpart cases as in Phase IIIC were included in the U.S. analysis. As for the uncertainty in T_n based on the T6&T7 method, the spread, $\pm\sigma_i$, around the uncertainty u_i, is larger in the U.S. case due to the larger statistical errors encountered in the Monte Carlo calculations of T_6 and T_7.

The Gaussian distributions that approximate the constructed NDFs based on the U.S. and the JAERI cases are shown in Figs. 39 and 40, respectively. The pertaining statistical parameters are summarized in Table VI. The mean prediction uncertainties are positive (calculated T_n is on the average larger than measurement) in all the measuring methods except in the (T6&T7) method in JAERI's case. The largest overprediction (by ~9.6%) in the U.S. calculations is obtained with the Li-pellet method (see Fig. 40) and the least is with zonal method (by ~1.7%). The corresponding values obtained for JAERI are ~5.4% (Li-pellet method) and about −2.4% (T6&T7 method). The negative value obtained with the T6&T7 method in JAERI's case is a result of the slight overprediction in T_6 attainable with the Li-glass method (see Table II) and the underprediction in T_7 attainable with the NE213 method (see Table V). Thus, the largest divergence in the prediction uncertainties as obtained by various measuring techniques is ~11% (U.S.) and ~8% (JAERI). When all cases with each measuring method are combined, the prediction uncertainty in T_n is ~4% (U.S.) and 1% (JAERI). These values are comparable to the mean prediction uncertainty in T_7 (see Table V) and T_6 (see Table II) obtained when no distinction is made between the various measuring methods. The spread, $\pm\sigma$, around these uncertainties is ~7% as can be seen from Table VI.

V.D.1. Design Safety Factors

The required design safety factors are shown in Figs. 41 and 42 based on the U.S. calculations and JAERI's calculations, respectively. If no safety factors are used ($S_k = 1$), the confidence levels based on the composed, zonal, Li-pellet, (T6&T7), and on all measuring methods are as follows:

~25, ~37, ~0, ~35, and ~28% (U.S.)
~36, ~26, ~25, ~65, and ~46% (JAERI)
~36, ~37, ~16, ~50, and ~38% (U.S.&JAERI).

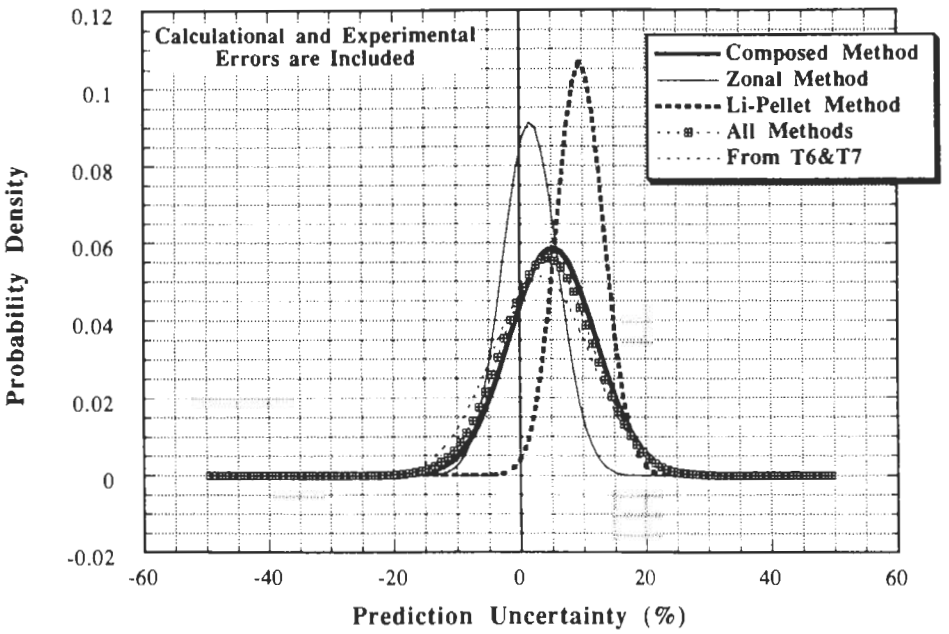

Fig. 39. Gaussian distributions that approximate the NDFs of the prediction uncertainties in T_n measured by several methods (U.S. calculations).

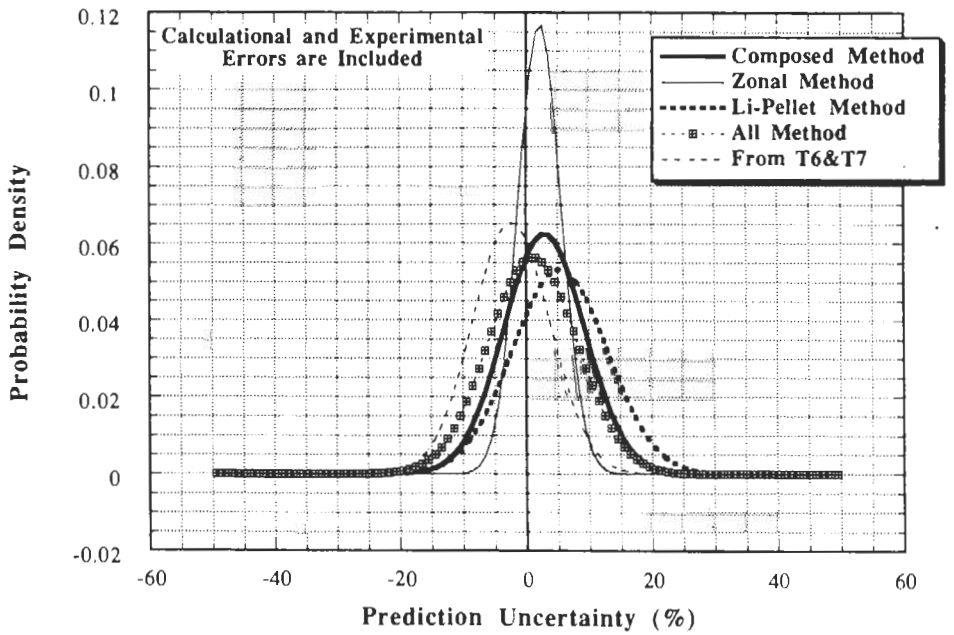

Fig. 40. Gaussian distributions that approximate the NDFs of the prediction uncertainties in T_n measured by several methods (JAERI calculations).

The confidence levels attainable in JAERI's case are larger than in the U.S. case. Combining the U.S. and JAERI's cases resulted in intermediate levels; however, all confidence levels are either below or equal 50% [except with the (T6&T7) method, JAERI], indicating that, on the average, the calculated T_n is larger than the actual measured value. At the highest confidence level, the most conservative safety factors based on the composed, zonal, Li-pellet, (T6&T7), and all measuring methods are as follows:

1.20, 1.10, 1.20, 1.26, and 1.26 (U.S.)
1.20, 1.10, 1.20, 1.16, and 1.20 (JAERI)
1.20, 1.10, 1.20, 1.26, and 1.26 (U.S.&JAERI).

TABLE VI

Statistical Parameters of the Prediction Uncertainty, u (%), of TPR from Natural Lithium (T_n) as Obtained from Various Experimental Methods

Method	Calculational and Experimental Errors Included			Calculational Errors Only Included		
	U.S.	JAERI	U.S. & JAERI	U.S.	JAERI	U.S. & JAERI
Composed						
Number of cases considered	9	17	26	9	17	26
$\bar{u}$ (average)	5.25	2.92	3.75	5.69	3.82	4.5
σ_u (standard deviation)	6.80	6.39	6.63	6.49	5.58	6.0
u_{rms} (root mean square)	8.59	7.02	7.62	8.63	6.76	7.5
u_{mp} (most probable)	5.0	2.5	5.0	−2.5	2.5	5.0
Zonal						
Number of cases considered	10	9	19	10	9	19
$\bar{u}$ (average)	1.71	2.17	1.91	1.56	1.25	1.43
σ_u (standard deviation)	4.37	3.40	3.98	4.41	2.98	3.86
u_{rms} (root mean square)	4.69	4.03	4.41	4.68	3.23	4.12
u_{mp} (most probable)	2.5	2.5	2.5	2.5	2.5	2.5
Li-pellet						
Number of cases considered	8	16	24	8	16	24
$\bar{u}$ (average)	9.61	5.36	6.85	9.17	4.72	6.5
σ_u (standard deviation)	3.74	7.49	6.74	3.12	7.49	6.51
u_{rms} (root mean square)	10.31	9.21	9.61	9.68	8.86	9.20
u_{mp} (most probable)	10.0	7.5	7.5	7.5	7.5	7.5
T_6 (Li-glass) + T_7 (NE213)						
Number of cases considered	33	38	71	33	38	71
$\bar{u}$ (average)	3.33	−2.36	0.40	2.74	−2.63	0.12
σ_u (standard deviation)	7.76	6.09	7.51	7.63	6.47	7.58
u_{rms} (root mean square)	8.45	6.53	7.52	8.11	6.98	7.58
u_{mp} (most probable)	2.5	−2.5	−2.5	−2.5	−7.5	−7.5
All methods						
Number of cases considered	***60***	***80***	***140***	60	80	140
$\bar{u}$ (average)	***4.35***	***1.03***	***2.50***	3.86	0.76	2.24
σ_u (standard deviation)	***7.11***	***7.08***	***7.29***	6.89	6.95	7.10
u_{rms} (root mean square)	***8.34***	***7.15***	***7.70***	7.90	7.00	7.44
u_{mp} (most probable)	***2.5***	***−2.5***	***2.5***	7.5	2.5	7.5
	1.26	***1.2***	***1.26***	1.20	1.16	1.2

These factors are similar in JAERI and the U.S. cases, except with the (T6&T7) method where the required safety factor is lower in JAERI's case than in the U.S. case.

V.D.2. Effect of Calculational Methods Applied

Figures 43 and 44 give the NDF and the approximating Gaussian curves of the prediction uncertainty based on the independent DO and MC calculations of the U.S. and JAERI, respectively. Figures 45 and 46 show the required safety factors as obtained from the DO method, the MC method, and from results based on both methods. The statistical parameters ($\bar{u}$, σ_u, etc.) are given in Table III and the safety factors are also summarized in Table IV for several confidence levels. These parameters are given for the case when all the measuring techniques are considered together.

The mean value, $\bar{u}$, of T_n based on the DO and MC method in the U.S. calculations is ~6.5% and ~2.3%, respectively, with a spread, σ_u, of ~6.8% in both cases. Note that the values of the corresponding parameters in the case of combining the results from the two methods are intermediate [$\bar{u} = 4.5\%$, $\sigma_u = 7\%$] as shown in Table VI. Again, the DO method tends to give larger prediction uncertainties than the ones obtained from the MC method by ~4%, leading to larger safety factors at various confidence levels. As can be seen from

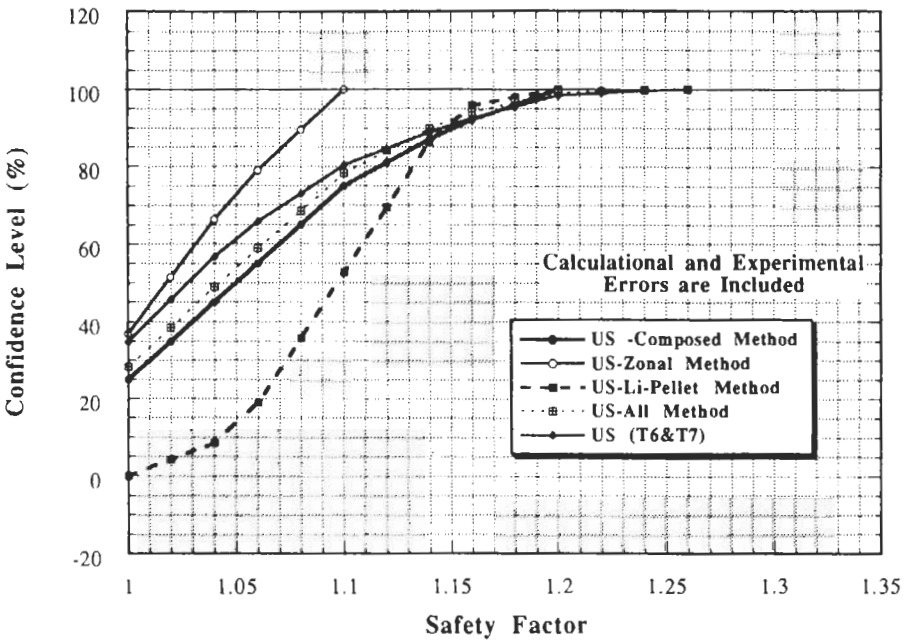

Fig. 41. Confidence level that calculations will not exceed measurements as a function of the design safety factor for T_n (U.S. calculations—all phases).

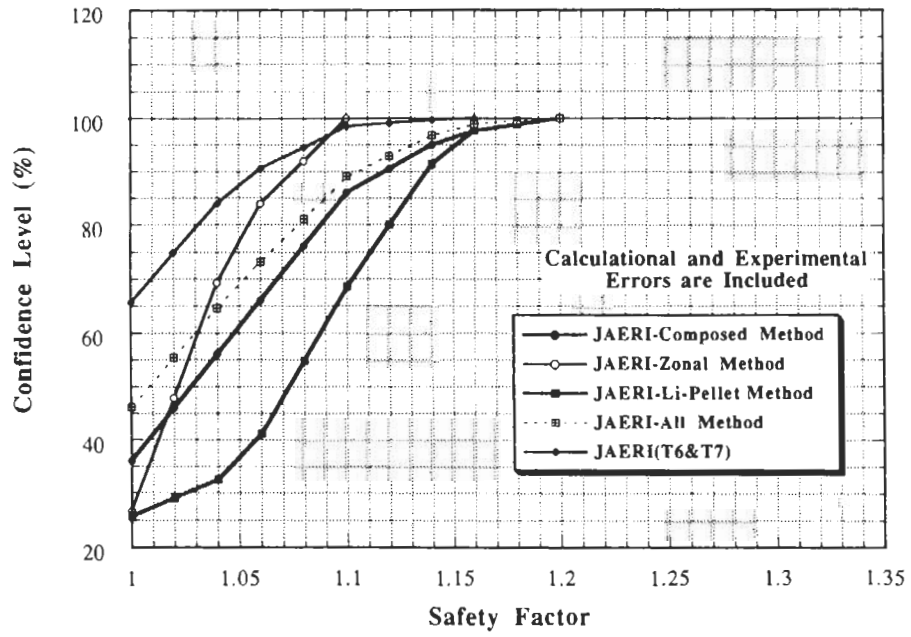

Fig. 42. Confidence level that calculations will not exceed measurements as a function of design safety factor for T_n (JAERI's calculations—all phases).

Table IV, the safety factors are lower than those calculated for T_6 by ~2% up to a confidence level of ~90% beyond which they are lower by ~5 to 7%. These features are the same when JAERI's calculations are considered but the safety factors calculated in this case are lower than those of the U.S. by ~3 to 4%.

V.E. Effect of Variations in Geometrical Arrangement and Incident Neutron Spectrum on the Prediction Uncertainty of TPR

Since the geometrical configuration and the conditions of the incident source are different between

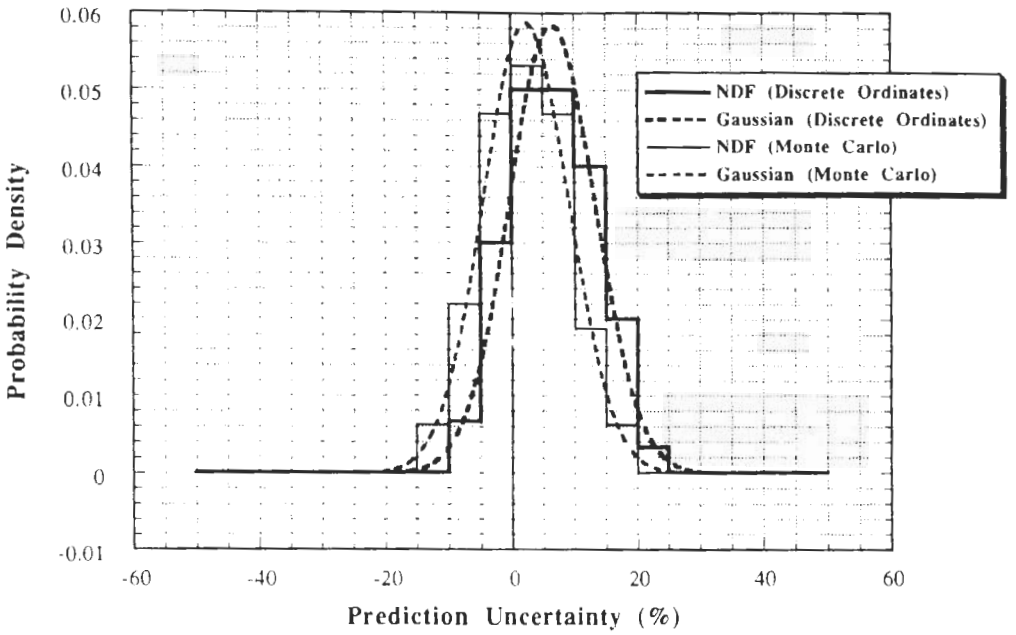

Fig. 43. Normalized density functions of the prediction uncertainties in T_n constructed from the DO and MC calculations (U.S. calculations, all measuring methods, all phases).

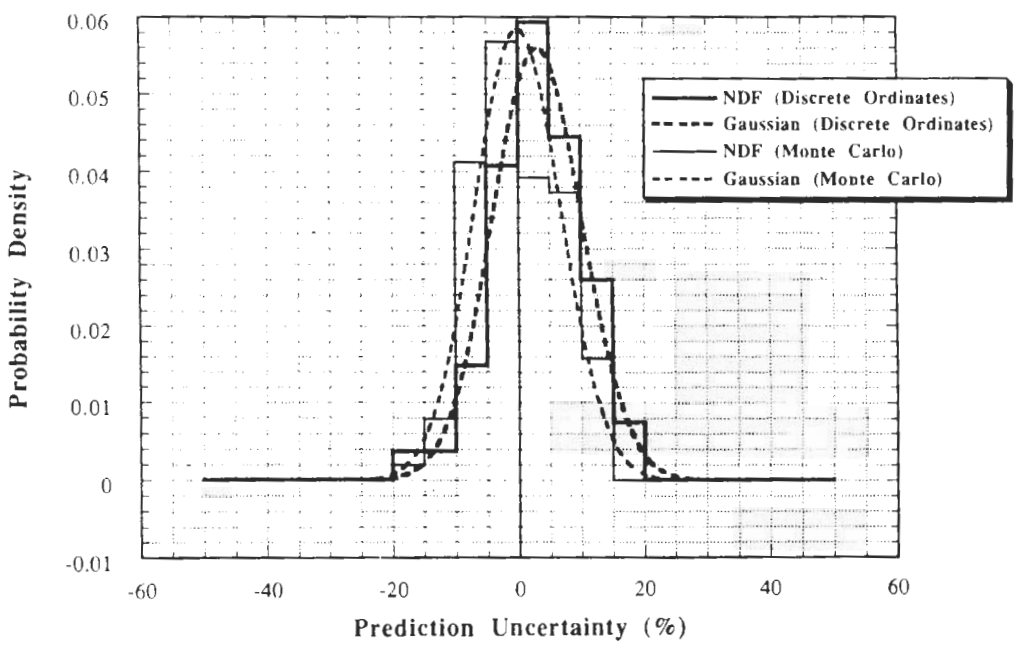

Fig. 44. Normalized density functions of the prediction uncertainties in T_n constructed from the DO and MC calculations (JAERI calculations, all measuring methods, all phases).

Phases I, II, and III, the prediction uncertainty in TPR and the required safety factors were calculated in each phase and compared to the corresponding values when all phases are considered simultaneously. Table VII gives the pertaining uncertainty parameters and Figs. 47, 48, and 49 give the required safety factors in each phase for T_6, T_7, and T_n, respectively.

By examining Table VII, it can be seen that the prediction uncertainty $\bar{u}$ is noticeably different in Phase I as compared to other phases. For example, in the U.S.

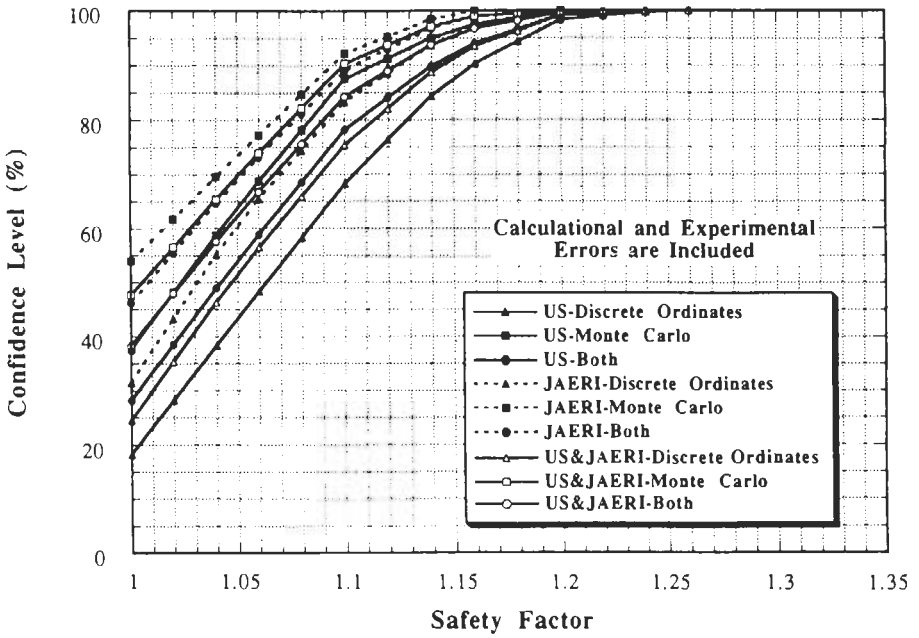

Fig. 45. Effect of the calculational method on the confidence levels and safety factors (T_n—all methods—all phases).

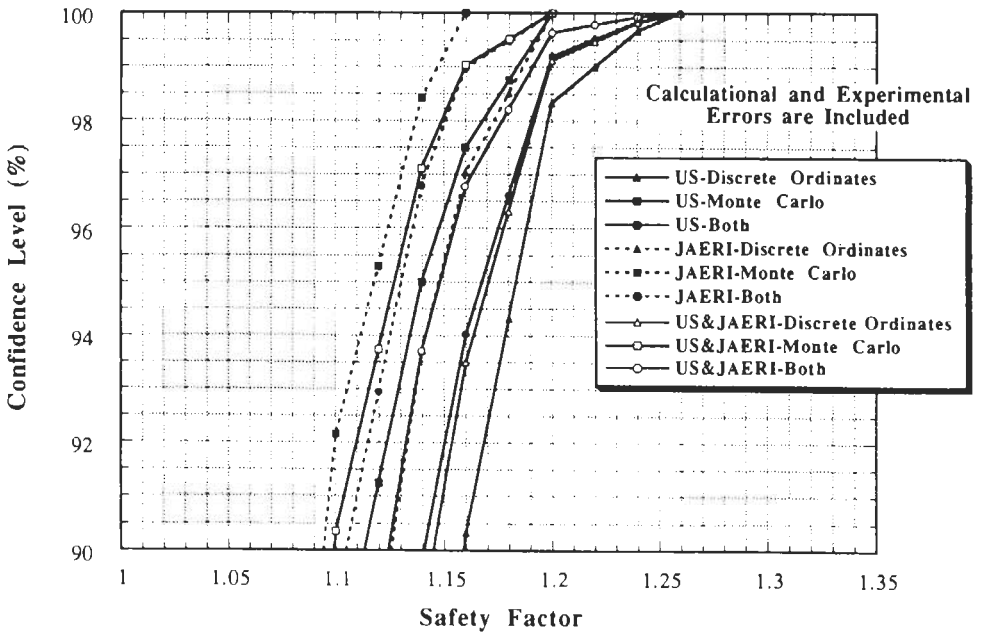

Fig. 46. Effect of the calculational method on the confidence levels and safety factors (T_n—all methods—all phases—confidence levels above 90%).

calculations, the uncertainties ū's are positive and large in Phase I for T_6, T_7, and T_n (ū = ~15%, ~14%, and ~12%) as compared to the corresponding uncertainties in Phase II and Phase III, which are alsc positive but have smaller values of ~4% (T_6), ~1 to 5% (T_7), and ~2 to 5% (T_n). Likewise, in JAERI's calculations of Phase I, the uncertainties ū's are negative and have large absolute values (except for T_7) of about −4% (T_6) and about −7% (T_n) compared to the uncertainties found in other phases. As pointed out in Refs. 7, 32, and 33, large discrepancies between calculations and measurements were identified, particularly for local

TABLE VII

Statistical Parameters of the Prediction Uncertainty, u (%), of TPR and Dependence on Geometry and Incident Neutron Spectrum

(All calculational and experimental methods are considered.)

Parameter	U.S.				JAERI				U.S. & JAERI			
	P1[a]	P2[a]	P3[a]	All[a]	P1[a]	P2[a]	P3[a]	All[a]	P1[a]	P2[a]	P3[a]	All[a]
T6 (all methods)												
Number of cases considered	11	55	20	*86*	8	51	36	*95*	19	106	56	*181*
$\bar{u}$ (mean)	14.56	3.84	4.50	*4.95*	−4.42	2.11	3.13	*2.09*	6.33	3.07	3.66	*3.52*
σ_u (standard deviation)	8.59	9.04	7.55	*9.14*	11.01	8.88	6.58	*8.39*	13.52	9.01	7.00	*8.89*
Safety factor (100% confidence)[b]	1.30	1.35	1.20	*1.35*	1.20	1.35	1.20	*1.35*	1.30	1.35	1.20	*1.35*
T7 (all methods)												
Number of cases considered	10	45	24	*79*	8	42	39	*89*	18	87	63	*168*
$\bar{u}$ (mean)	14.30	5.30	0.92	*5.11*	−1.25	−1.50	0.90	*−0.36*	7.39	2.23	0.91	*2.28*
σ_u (standard deviation)	8.23	10.77	8.78	*10.69*	7.40	7.73	11.11	*9.50*	11.03	10.11	10.30	*10.46*
Safety factor (100% confidence)	1.35	1.30	1.26	*1.35*	1.16	1.16	1.30	*1.30*	1.35	1.30	1.30	*1.35*
Tn (all methods)												
Number of cases considered	6	26	28	*60*	6	24	50	*80*	12	50	78	*140*
$\bar{u}$ (mean)	12.05	2.40	4.53	*4.35*	−6.59	0.30	2.12	*1.03*	2.73	1.44	3.04	*2.50*
σ_u (standard deviation)	6.89	5.67	7.22	*7.11*	7.01	5.53	7.09	*7.08*	11.63	5.70	7.24	*7.29*
Safety factor (100% confidence)	1.26	1.20	1.20	*1.26*	1.06	1.16	1.20	*1.20*	1.26	1.20	1.20	*1.26*

[a]P1 = Phase I; P2 = Phase II; P3 = Phase III; All = all phases.
[b]See footnote of Table III.

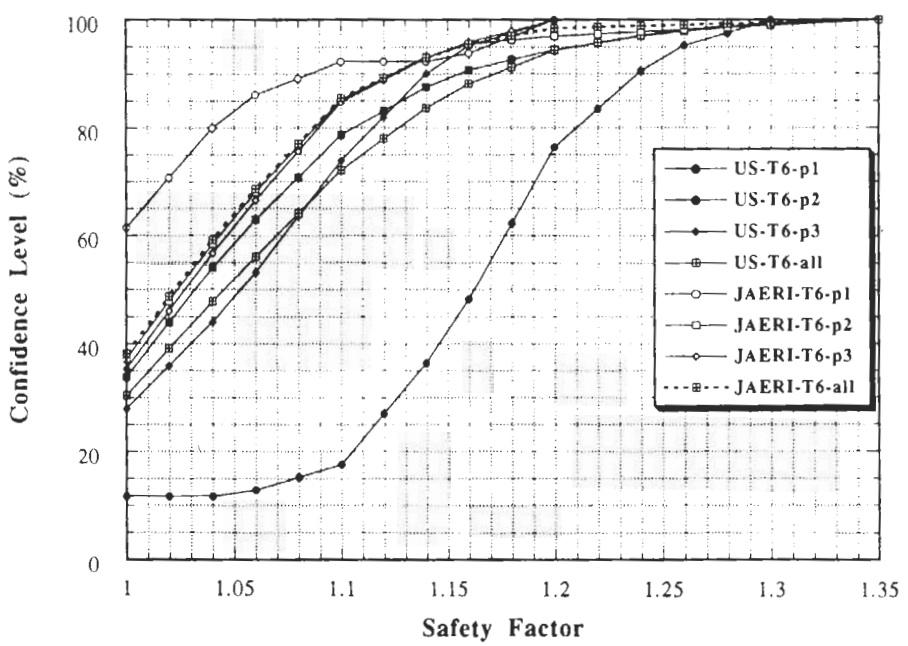

Fig. 47. Effect of the geometry and incident spectrum in each phase on the confidence levels and safety factors (T_6 – all methods – all phases).

T_6, due to the large uncertainty in predicting the low-energy component of the incident neutron source. Several sources contributed to this uncertainty, among which are the difficulty in accurately modeling the complicated neutron target and room walls, the source separation model used in the Monte Carlo calculations,[5] and the uncertainties in determining the exact atomic densities of the concrete walls of the room where the

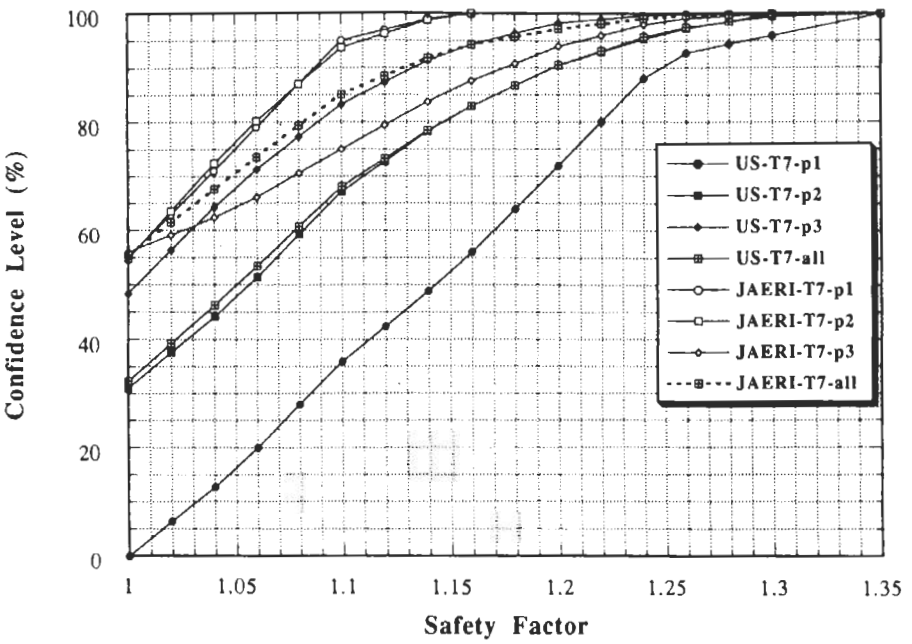

Fig. 48. Effect of the geometry and incident spectrum in each phase on the confidence levels and safety factors (T_7—all methods—all phases).

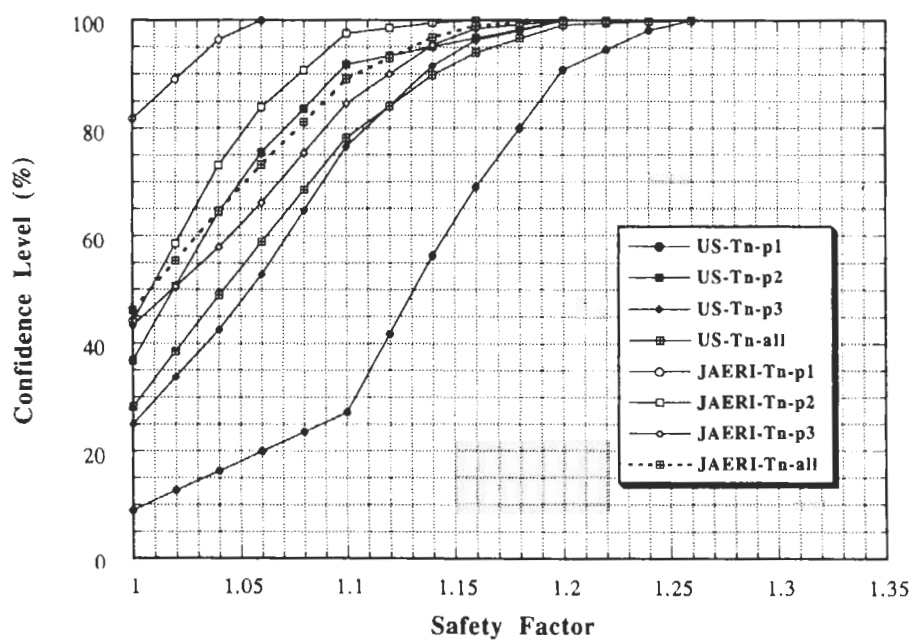

Fig. 49. Effect of the geometry and incident spectrum in each phase on the confidence levels and safety factors (T_n—all methods—all phases).

experiments were performed. The situation is different in Phase II (closed geometry) and Phase III (simulated line source) where the uncertainties in determining the neutron room-return component of the incident neutron source and the difficulty in modeling the concrete wall of the large room were eliminated.

To be noted from Table VII is that in the U.S. calculations, the difference between the prediction uncertainty $\bar{u}$ in Phase II and Phase III is within ~1 to 2% (T_6, T_n) and ~4% (T_7). In JAERI's calculations, this difference is ~1 to 2% for T_6, T_7, and T_n. Therefore, by changing the configuration from a rectangular

enclosure with the source located at one side of the test assembly to an annular assembly surrounding a simulated line source, the prediction uncertainty of TPR, in general, has only changed by ~1 to 4%. Note also that the difference between the standard deviations, σ_u's, in the uncertainty of T_6, T_7, and T_n in the two phases is ~2 to 3%, which is within the change in the prediction uncertainties, $\bar{u}$'s.

VI. SUMMARY

Over a dozen distinctive experiments have been performed within the U.S.DOE/JAERI collaborative program on fusion neutronics to quantify the uncertainty involved in the prediction of TPR, as a prime parameter in the fusion blanket. In this regard, various codes and nuclear data were used in analyzing these experiments in addition to applying various measuring techniques for cross-checking experimental results. The experiments proceeded from a simple, one material test assembly to a more prototypical assembly that included the engineering features of a fusion blanket (first wall, coolant channels, multiplier . . .). Furthermore, the neutron source conditions were altered in these experiments to closely simulate those conditions found in tokamak plasmas.

In this paper, the calculational and experimental uncertainties (errors) in local TPR in each experiment, i, were propagated and thus contributed to the prediction uncertainty, u_i, in the line-integrated TPR and its standard deviation, σ_i. The uncertainties in the line-integrated TPR were examined rather than examining the uncertainties in local values since they would be more representative to the uncertainties in TBR found in fusion reactors. The latter was previously studied.[32,33] An approach was also outlined in this work that gives estimates to the prediction uncertainty in the volume-integrated TPR based on measurements and calculations of local TPR in the traverse direction. It was shown that the difference between the prediction uncertainty of the line-integrated and volume-integrated TPR is within a few percent for the cases considered, indicating that the assessment of the design margins from the results of the line-integrated TPR could be applied as well to TBR. A novel methodology was developed (see Ref. 3) to arrive at estimates to design safety factors that fusion blanket designers can use to ensure that the achievable TBR in a blanket does not fall below a minimum required value. The methodology was applied to construct NDFs from the prediction uncertainties, u_i's, and their associated deviations, σ_i's, calculated for all the experiments carried out during the program. Important statistical parameters were calculated from the NDFs, such as the global mean prediction uncertainty, $\bar{u}$, and the possible spread, $\pm\sigma_u$, around it. The design safety factors were then derived from these NDFs, and they account for the discrepancies found between various calculational methods (e.g., discrete ordinates and Monte Carlo) and measured values based on various experimental techniques. Associated with each safety factor is a confidence level, which designers may choose to have, that calculated TPR will not exceed the actual measured value. Tabular and graphical forms for these factors are also given as derived independently for TPR from Li-6 (T_6), Li-7 (T_7), and natural lithium (T_n). Furthermore, distinction was made between safety factors based on the U.S. calculations, JAERI's calculations, and both calculations considered simultaneously.

Based on considering all calculational and experimental methods used, the prediction uncertainty, $\bar{u}$, in line-integrated T_6 is ~5% (U.S.) and ~2% (JAERI) with standard deviation, $\pm\sigma_u$, of ~8 to 9%. However, when these uncertainty parameters are derived independently for each measuring technique, the divergence among them is ~8% in estimating $\bar{u}$, which is within the deviation $\pm\sigma_u$. If calculational methods are considered independently, it was shown in the U.S. and the JAERI calculations that the DO methods tend to give larger uncertainties (by ~5%) than those based on MC calculations. In this case, $\bar{u}$ = ~8% (DO) and ~2.6% (MC) based on the U.S. calculations. As for JAERI, $\bar{u}$ = ~5% (DO) and ~0.2% (MC). Accordingly, the associated safety factors at the various confidence levels are ~3 to 6% (U.S.) and 2 to 5% (JAERI) larger with the DO method than those of the MC method. Not using safety factors by designers (S_k = 1), the probability that the calculated T_6 will exceed the actual value is ~70% (U.S.) and ~62% (JAERI). To achieve the highest confidence level that calculated T_6 does not exceed the actual value, the safety factor to be used by designers is ~1.35. At lower confidence levels, the safety factors based on the U.S. calculations are larger than those based on JAERI's calculations by ~2 to 5%.

The mean prediction uncertainty, $\bar{u}$, in the line-integrated T_7 based on considering all calculational and experimental techniques is ~5% (U.S.) and about −0.4% (JAERI) with a spread, $\pm\sigma_u$, of ~11% (U.S.) and ~9% (JAERI). The divergence among the various measuring techniques is ~14% (U.S.) and ~22% (JAERI), which is larger than the standard deviation σ_u, indicating the need to further examine these techniques in measuring TPR. The DO method gives larger uncertainties (by ~6%) than the MC method used in the U.S. calculations [$\bar{u}$ ~9% (DO) and ~02% (MC)], while they are comparable in JAERI's calculations [$\bar{u}$ ~ −0.9% (DO) and ~0.02% (MC)] within 1%. If no safety factors are used by designers, the chance that the calculated T_7 will exceed the actual value is ~68% (U.S.) and ~45% (JAERI). To ensure that calculations are lower than actual values for T_7, the safety factor to be applied is ~1.35 (U.S.) and ~1.30 (JAERI).

The mean prediction uncertainty, $\bar{u}$, in the line-integrated TPR from natural lithium (T_n) is ~4% (U.S.) and ~1% (JAERI). The estimated deviation

around the mean value, $\pm\sigma_u$, is ~7%. The divergence among the various measuring techniques used is ~11% (U.S.) and ~8% (JAERI), which is larger than the standard deviation σ_u. In the MC and DO calculations performed by the U.S. and JAERI, the prediction uncertainties estimated from the DO calculations are larger than the ones based on the MC methods by ~4% [U.S.: $\bar{u}$ ~ 6.5% (DO) and ~2.3% (MC); JAERI: $\bar{u}$ ~ 3.1% (DO) and about −0.05% (MC)]. Without applying a safety factor to T_n calculations, the probability that the calculated values are larger than measurements is ~72% (U.S.) and 54% (JAERI). Applying a safety

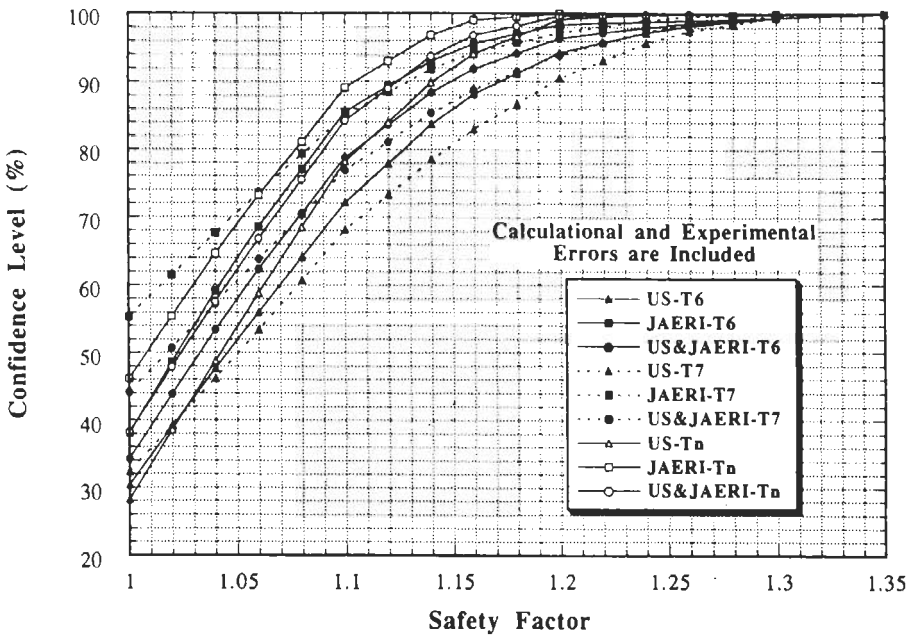

Fig. 50. Confidence level that calculations will not exceed measurements as a function of design safety factor for T_6, T_7, and T_n (all methods—all phases).

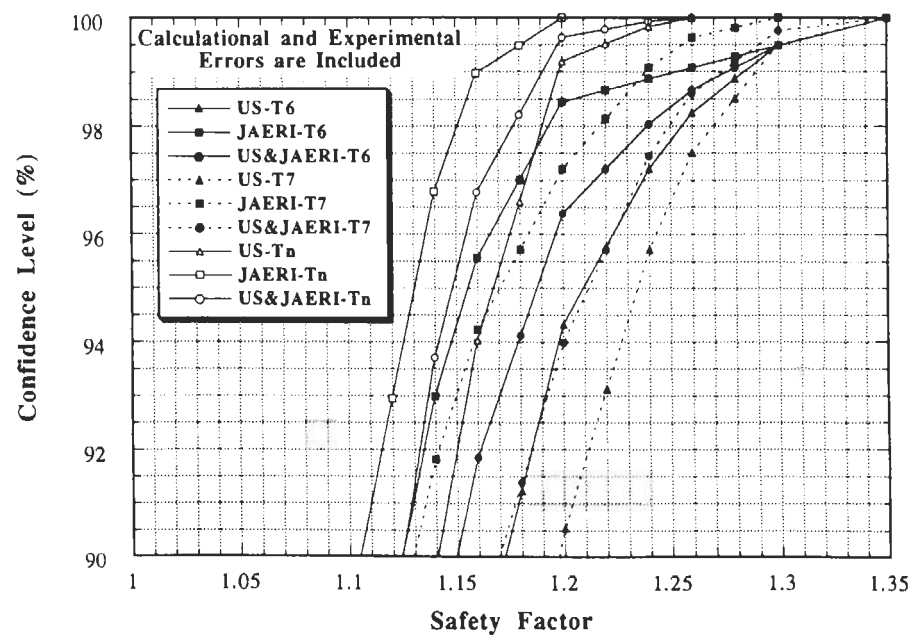

Fig. 51. Confidence level that calculations will not exceed measurements as a function of design safety factor for T_6, T_7, and T_n (all methods—all phases—confidence levels above 90%).

factor of ~1.26 (U.S.) and ~1.20 (JAERI) will ensure that calculations are indeed below actual values.

Figures 50 and 51 along with Table IV can be used by blanket designers to obtain the required safety factors for a wide range of confidence levels, which could be applied to the calculations of T_6, T_7, and T_n. For practical purposes, a confidence level of ~95% could be applied as an upper limit, as is the case in many engineering design applications. It should be emphasized, however, that these factors are applicable to the TPR in Li_2O breeding material as obtained from the U.S. DOE/JAERI collaborative program based on simplified prototypical fusion blanket assemblies under very ideal neutron source conditions. It is needless to say that when experiments will be conducted in a much more realistic fusion neutron environment, to meet more stringent R&D requirements, the applicable safety factors are going to be larger than what have been reported here. Nevertheless, the results cited in this paper can be used as initial guidance to assist blanket designers in resolving tritium self-sufficiency issues in their designs.

ACKNOWLEDGMENT

This work was conducted under the U.S. Department of Energy grant DOE-FG03-88ER52150.

REFERENCES

1. M. A. ABDOU, E. L. VOLD, C. Y. GUNG, M. Z. YOUSSEF, and K. SHIN, "Deuterium-Tritium Fuel Self-Sufficiency in Fusion Reactors," *Fusion Technol.*, **9**, 250 (1986).

2. M. Z. YOUSSEF and M. A. ABDOU, "Uncertainties in Prediction of Tritium Breeding in Candidate Blanket Designs Due to Present Uncertainties in Nuclear Data Base," *Fusion Technol.*, **9**, 286 (1986).

3. M. Z. YOUSSEF, A. KUMAR, M. A. ABDOU, Y. OYAMA, and H. MAEKAWA, "Fusion Integral Experiments and Analysis and the Determination of Design Safety Factors—I: Methodology," *Fusion Technol.*, **28**, 366 (1995).

4. T. NAKAMURA and M. A. ABDOU, "Summary of Recent Results from the JAERI/U.S. Fusion Neutronics Phase I Experiments," *Fusion Technol.*, **10**, 541 (1986).

5. M. Z. YOUSSEF, C. GUNG, M. NAKAGAWA, T. MORI, K. KOSAKO, and T. NAKAMURA, "Analysis and Intercomparison for Phase I Fusion Integral Experiments at the FNS Facility," *Fusion Technol.*, **10**, 549 (1986).

6. M. Z. YOUSSEF et al., "Phase I Fusion Integral Experiments, Vol. II: Analysis," UCLA-ENG-88-15, University of California, Los Angeles (Sep. 1988); see also JAERI-M-88-177, Japan Atomic Energy Research Institute (Aug. 1988).

7. M. Z. YOUSSEF, Y. WATANABE, C. Y. GUNG, M. NAKAGAWA, T. MORI, and K. KOSAKO, "Analysis of Neutronics Parameters Measured in Phase II Experiments of the JAERI/U.S. Collaborative Program on Fusion Blanket Neutronics, Part II: Tritium Production and In-System Spectrum," *Fusion Eng. Des.*, **9**, 323 (1989).

8. M. NAKAGAWA et al., "Analysis of Neutronics Parameters Measured in Phase II Experiments of JAERI/U.S. Collaborative Program on Breeder Neutronics, Part I: Source Characteristics and Reaction Rate Distribution," *Fusion Eng. Des.*, **9**, 315 (1989).

9. Y. OYAMA, K. TSUDA, S. YAMAGUCHI, Y. IKEDA, C. KONNO, H. MAEKAWA, and T. NAKAMURA, "Phase II Experimental Results of JAERI/USDOE Collaborative Program on Fusion Blanket Neutronics Experiments," *Fusion Eng. Des.*, **9**, 309 (1989).

10. Y. OYAMA et al., "Phase-IIB Experiment of JAERI/USDOE Collaborative Program on Fusion Blanket Neutronics," *Fusion Technol.*, **15**, 1293 (1989).

11. M. Z. YOUSSEF, Y. WATANABE, M.A. ABDOU, M. NAKAGAWA, T. MORI, K. KOSAKO, and T. NAKAMURA, "Comparative Analysis for Phase IIA and IIB Experiments of the U.S./JAERI Collaborative Program on Fusion Blanket Neutronics," *Fusion Technol.*, **15**, 1299 (1989).

12. Y. IKEDA, C. KONNO, Y. OYAMA, K. OISHI, and T. NAKAMURA, "Determination of Neutron Spectrum in D-T Fusion Field by Foil Activation Technique," *Fusion Technol.*, **15**, 1287 (1989).

13. M. Z. YOUSSEF, M. A. ABDOU, Y. WATANABE, and P. M. SONG, "The U.S./JAERI Collaborative Program on Fusion Neutronics; Phase IIA and IIB Fusion Integral Experiments, The U.S. Analysis," UCLA-ENG-90-14, University of California at Los Angeles (Dec. 1989).

14. M. NAKAGAWA, T. MORI, K. KOSAKO, Y. OYAMA, and T. NAKAMURA, "JAERI/U.S. Collaborative Program on Fusion Blanket Neutronics, Analysis of Phase IIA and IIB Experiments," JAERI-M-89-154, Japan Atomic Energy Research Institute (Oct. 1989).

15. Y. OYAMA et al., "Phase IIA and IIB Experiments of JAERI/U.S. DOE Collaborative Program of Fusion Blanket Neutronics—Neutronics Measurements on Beryllium Configuration—in a Full-Coverage Blanket Geometry," JAERI-M-89-215, Pts. I and II, Japan Atomic Energy Research Institute (Dec. 1989).

16. M. Z. YOUSSEF, A. KUMAR, M. ABDOU, M. NAKAGAWA, K. KOSAKO, Y. OYAMA, and T. NAKAMURA, "Analysis for Heterogeneous Blankets and Comparison to Measurements: Phase IIC Experiments of the USDOE/

JAERI Collaborative Program on Fusion Neutronics," *Fusion Technol.*, **19**, 1891 (1991).

17. Y. OYAMA et al., "Measured Characteristics of Be Multi-Layered and Coolant Channel Blankets: Phase IIC Experiments of the JAERI/USDOE Collaborative Program on Fusion Neutronics," *Fusion Technol.*, **19**, 1955 (1991).

18. Y. OYAMA et al., "Phase-IIC Experiments of the USDOE/JAERI Collaborative Program on Fusion Blanket Neutronics—Experiments and Analysis of the Heterogeneous Fusion Blankets, Volume I: Experimental Results," JAERI-M-92-182, Japan Atomic Energy Research Institute (Dec. 1992); see also UCLA-FNT-63, UCLA-ENG-93-18, University of California at Los Angeles (Dec. 1992).

19. M. Z. YOUSSEF et al., "Phase-IIC Experiments of the USDOE/JAERI Collaborative Program on Fusion Blanket Neutronics—Experiments and Analysis of the Heterogeneous Fusion Blankets, Volume II: Analysis," UCLA-FNT-64, UCLA-ENG-93-19, University of California at Los Angeles (Dec. 1992); see also M. NAKAGAWA et al., JAERI-M-92-183, Japan Atomic Energy Research Institute (Dec. 1992).

20. A. KUMAR, Y. WATANABE, and M. YOUSSEF, "Analysis for the Selection of Experimental Configurations for Heterogeneity and Be Multi-Layered Experiments of U.S.DOE/JAERI Collaborative Program on Blanket Neutronics," *Fusion Technol.*, **15**, 1309 (1989).

21. M. Z. YOUSSEF et al., "Nuclear Analysis of Integral Experiments on a Li_2O Test Assembly with Local Heterogeneities Utilizing a 14-MeV Neutron Source," *Fusion Technol.*, **28**, 243 (1995).

22. Y. OYAMA et al., "Neutronics Integral Experiments of Lithium-Oxide Fusion Blanket with Heterogeneous Configurations Using Deuterium-Tritium Neutrons," *Fusion Technol.*, **28**, 216 (1995).

23. T. NAKAMURA et al., "A Line D-T Neutron Source Facility for Annular Blanket Experiment: Phase III of the JAERI/USDOE Collaborative Program on Fusion Neutronics," *Fusion Technol.*, **19**, 1873 (1991).

24. Y. OYAMA et al., "Annular Blanket Experiment Using a Line DT Neutron Source: Phase IIIA of the JAERI/USDOE Collaborative Program on Fusion Neutronics," *Fusion Technol.*, **19**, 1879 (1991).

25. M. Z. YOUSSEF, Y. WATANABE, A. KUMAR, Y. OYAMA, and K. KOSAKO, "Analysis for the Simulation of a Line Source by a 14 MeV Moving Point Source and Impact on Blanket Characteristics: The USDOE/JAERI Collaborative Program on Fusion Neutronics," *Fusion Technol.*, **19**, 1843 (1991).

26. C. KONNO et al., "Measurements of the Source Term for Annular Blanket Experiment with a Line Source: Phase IIIA of JAERI/USDOE Collaborative Program on Fusion Neutronics," *Fusion Technol.*, **19**, 1885 (1991).

27. Y. OYAMA et al., "Phase III Experimental Results of JAERI/USDOE Collaborative Program on Fusion Neutronics," *Fusion Eng. Des.*, **18**, 203 (1991).

28. M. Z. YOUSSEF, A. KUMAR, M. A. ABDOU, Y. OYAMA, K. KOSAKO, and T. NAKAMURA, "Post-Analysis for the Line Source Phase IIIA Experiments of the USDOE/JAERI Collaborative Program on Fusion Neutronics," *Fusion Eng. Des.*, **18**, 265 (1991).

29. M. Z. YOUSSEF et al., "The Nuclear Analysis of an Annular Li_2O Blanket System Surrounding an Artificially Simulated 14-MeV Line Source and Comparison of Calculations to Measurements," *Fusion Technol.*, **28**, 320 (1995).

30. Y. OYAMA et al., "Phase III Experiments of the JAERI/USDOE Collaborative Program on Fusion Blanket Neutronics: Line Source and Annual Blanket Experiments, Volume I: Experiments," JAERI-M-94-015, Japan Atomic Energy Research Institute (Feb. 1994); see also, M. Z. YOUSSEF, UCLA-FNT-75, UCLA-ENG-93-85, University of California, Los Angeles (1995).

31. M. Z. YOUSSEF et al., "Phase III Experiments of the JAERI/USDOE Collaborative Program on Fusion Blanket Neutronics: Line Source and Annual Blanket Experiments, Volume II: Analysis" (to be published) (1995).

32. M. Z. YOUSSEF, A. KUMAR, and M. A. ABDOU, "The Prediction Capability for Tritium Production and Other Reaction Rates in Various Systems Configurations for a Series of the USDOE/JAERI Collaborative Fusion Blanket Experiments," *Fusion Eng. Des.*, **18**, 407 (1991).

33. Y. OYAMA, K. KOSAKO, M. NAKAGAWA, and T. NAKAMURA, "Comparative Study of Systems and Nuclear Data in C/E Ratio for a Series of JAERI/USDOE Collaborative Fusion Blanket Experiments," *Fusion Eng. Des.*, **18**, 281 (1991).

34. S. YAMAGUCHI et al., "An On-Line Method for Tritium Production Measurement with a Pair of Lithium-Glass Scintillators," *Nucl. Instrum. Methods*, **A245**, 413 (1987).

35. Y. OYAMA et al., "A Small Spherical NE213 Scintillation Detector for Use in In-Assembly Fast Neutron Spectrum Measurements," *Nucl. Instrum. Methods*, **A256**, 333 (1987).

36. LOS ALAMOS MONTE CARLO GROUP, "MCNP—A General Monte Carlo Code for Neutron and Photon Transport," Version 3A, LA-7396, Rev. 2, Los Alamos National Laboratory (1986).

37. W. A. RHOADES and R. L. CHILDS, "An Updated Version of the DOT 4 (Version 4.3) One-and-Two-Dimensional Neutron/Photon Transport Code," ORNL-5851, Oak Ridge National Laboratory (Apr. 1982); see also CCC-429, Radiation Shielding Information Center (1982).

38. L. P. KU and J. KOLIBAL, "RUFF—A Ray Tracing Program to Generate Uncollided Flux and First Collision Source Moments for DOT4: A User's Manual," EAD-R-16, Plasma Physics Laboratory, Princeton University (1980).

39. R. A. MacFARLANE, "TRANSX-CTR: A Code for Interfacing MATXS Cross-Section Libraries to Nuclear Transport Codes for Fusion Systems Analysis," LA-9863-MS, Los Alamos National Laboratory (Feb. 1984).

40. P. G. YOUNG and L. STEWART, "Evaluated Data for n+9Be Reactions," LA-7932-MS, Los Alamos National Laboratory (July 1979).

41. M. NAKAGAWA and T. MORI, "MORSE-DD, A Monte Carlo Code Using Multigroup Double Differential Form Cross-Sections," JAERI-M84-126, Japan Atomic Energy Research Institute (July 1984).

42. M. NAKAGAWA, T. MORI, and M. SASAKI, "Comparison of Vectorization Methods Used in a Monte Carlo Code," *Nucl. Sci. Eng.*, **107**, 58 (1991).

43. "DOT 3.5: Two-Dimensional Discrete Ordinates Radiation Transport Code," CCC-276, Radiation Shielding Information Center; see also W. A. RHOADES and F. R. MYNETT, "The DOT III Two-Dimensional Discrete Ordinates Transport Code," ORNL-TM-4280, Oak Ridge National Laboratory (Sep. 1973).

44. W. PRESS, B. FLANNERY, S. TEUKOLSKY, and W. VETTERLING, *Numerical Recipes: The Art of Scientific Computing*, Cambridge University Press, New York (1990).

45. P. LANCASTER and S. KESTUTIS, *Curve and Surface Fitting: An Introduction*, Academic Press, New York (1986).

46. Y. IKEDA and M. Z. YOUSSEF, "Two-Dimensional Cross-Section Sensitivity and Uncertainty Analysis for Tritium Production Rate in Fusion-Oriented Integral Experiments," *Fusion Technol.*, **13**, 616 (1988).

47. M. Z. YOUSSEF and Y. WATANABE, "Study on the Accuracy of Several Beryllium Evaluations and Comparison of Measured and Calculated Data on Reaction Rates and Tritium Production Distributions," *Fusion Technol.*, **19**, 1967 (1991).

48. P. M. SONG, M. Z. YOUSSEF, and M. ABDOU, "A New Approach and Computational Algorithm for Sensitivity/Uncertainty Analysis for SED and SAD with Application to Beryllium Integral Experiments," *Nucl. Sci. Eng.*, **113**, 339 (1993).

Mahmoud Z. Youssef (PhD, nuclear engineering, University of Wisconsin, 1980) is a senior research engineer in the Department of Mechanical, Aerospace, and Nuclear Engineering at the University of California, Los Angeles (UCLA). He participated in several conceptual magnetic fusion energy and inertial fusion energy reactor design studies with emphasis on nuclear analysis and blanket/shield design. His research interests are in the areas of blanket/shield design optimization, nuclear data, sensitivity/uncertainty studies, neutronics methods and code development, tritium fuel cycle, radioactivity and safety aspects of fusion, integral experiments, neutronics testing, and research and development for fusion reactors, particularly the International Thermonuclear Experimental Reactor (ITER).

Anil Kumar (PhD, University of Bombay, India, 1981) is senior development engineer at UCLA. His current research interests include fusion reactor nucleonics experiments and analysis, technique development for nuclear heating, decay heat measurements, biological dose, fusion diagnostics, safety factor methodology for fusion reactor design parameters, low-activation materials, inertial confinement fusion, and sequential reactions. He has conducted experiments at leading facilities such as the Fusion Neutronics Source (FNS) facility in Japan, the Tokamak Fusion Test Reactor (TFTR) at Princeton University, and LOTUS in Switzerland.

Mohamed A. Abdou is a professor in the Department of Mechanical, Aerospace, and Nuclear Engineering at UCLA and also is the director of fusion technology at UCLA. His research interests include neutronics, thermomechanics, fusion technology, and reactor design and analysis. He served as the U.S. leader of the Japan Atomic Energy Research Institute (JAERI)/U.S. Department of Energy (U.S. DOE) collaboration on fusion blanket neutronics.

Yukio Oyama (BS, physics, 1975; MS, nuclear physics, 1977; and Dr. Eng., 1989, Osaka University, Japan) is a principal scientist at JAERI. He has worked in the area of fusion neutronics experiments since 1978. He is currently involved in intense and high-energy neutron source projects.

Chikara Konno (MS, physics, Kyoto University, Japan, 1985) is a research scientist in the Department of Reactor Engineering at JAERI. He has worked

in the areas of fusion neutronics experiments, cross-section measurements, and neutron spectrum measurements using a proton-recoil counter.

Fujio Maekawa (MS, nuclear engineering, Osaka University, Japan, 1990) is a research scientist at JAERI. He has been engaged in integral experiments for fusion neutronics and studied the behavior of neutron, photon, and electron transport in media. His current interests are in the measurements of tritium and decay heat of irradiated materials.

Yujiro Ikeda (PhD, nuclear engineering, Nagoya University, Japan, 1981) is head of the Fusion Neutronics Laboratory in the Department of Reactor Engineering at JAERI. He has worked in the areas of fusion neutronics experiments, induced radioactivity experiment and analysis, direct nuclear heating measurements, activation cross-section measurements, and fusion dosimetry.

Kazuaki Kosako (BE, atomic engineering, Tokai University, Japan, 1984) has worked at Sumitomo Atomic Energy Industries since 1994. He worked in the Department of Reactor Engineering at JAERI from 1984 to 1992, where he was involved mainly in fusion neutronics. He is currently interested in the area of radiation damage of materials.

Masayuki Nakagawa (BS, 1965; MS, 1967; and PhD, 1979, nuclear engineering, Kyoto University, Japan) is a principal scientist in the Department of Reactor Engineering at JAERI. He is a head of the reactor system laboratory having the main responsibility for the computation method and design of reactors. He researched the development of neutronics computation methods and codes for fast reactors and fusion reactors and intelligent reactor design systems. His group has developed high-speed general-purpose Monte Carlo codes based on vector and/or parallel algorithms.

Takamasa Mori (BS, 1976; MS, 1979; and PhD, 1985, nuclear engineering, Kyoto University, Japan) is a principal scientist in the Department of Reactor Engineering at JAERI. He worked for the development of neutron transport codes using double-differential form cross sections. His research interests are in the field of reactor physics, especially the speedup of Monte Carlo calculation of high-energy particles based on vector and/or parallel algorithms.

Hiroshi Maekawa (BE, 1965; MS, 1967; and Dr. Eng., 1970, nuclear engineering, Tokyo Institute of Technology, Japan) is the deputy director of the Department of Reactor Engineering and the head of the Intense Neutron Source Laboratory at JAERI. He has worked on fusion neutronics for more than 20 years, and he planned and constructed the FNS facility. He served as the Japanese leader of the JAERI/U.S. DOE collaboration on fusion blanket neutronics. His recent research has focused on International Fusion Materials Irradiation Facility conceptual design activities.